

Forschungszentrum Karlsruhe
Technik und Umwelt

Wissenschaftliche Berichte
FZKA 5908

**Flow-induced Changes
of the Morphological Stability
in Directional Solidification:
Localized Morphologies**

L. Bühler, S. H. Davis

Institut für Angewandte Thermo- und Fluidodynamik

Juni 1997

Forschungszentrum Karlsruhe

Technik und Umwelt

Wissenschaftliche Berichte

FZKA 5908

Flow-induced changes of the morphological stability
in directional solidification:
localized morphologies

L. Bühler, S. H. Davis*

Institut für Angewandte Thermo- und Fluidodynamik

* Northwestern University, Evanston, USA

Forschungszentrum Karlsruhe GmbH, Karlsruhe

1997

Als Manuskript gedruckt
Für diesen Bericht behalten wir uns alle Rechte vor

Forschungszentrum Karlsruhe GmbH
Postfach 3640, 76021 Karlsruhe

ISSN 0947-8620

Flow-induced changes of the morphological stability in directional solidification: localized morphologies

Abstract

Steady, two-dimensional cellular convection is impressed upon a solid-liquid interface undergoing directional solidification. When the wave length $2\pi/\alpha$ of the convection is very long compared to that, $2\pi/\beta$, of the morphological instability, the interface is sheared by "parallel" remote flow periodic in the flow direction.

When the shear is taken to be constant instead of spatially periodic, a new formulation shows how a whole family of shear flows can be analyzed in a common way and how the physical mechanisms can be understood.

When the shear is spatially periodic, two new modes of response are identified. For α/β small and for small flow magnitude the morphological instability becomes localized near converging stagnation points. At the threshold the instability is steady and in a localized packet many morphological cells exist. For α/β not so small or for larger flow magnitudes, the morphological instability becomes localized near mid-points between stagnation points and the unstable interface pattern is travelling within a stationary envelope.

Strömungsbedingte Änderung der morphologischen Stabilität bei gerichteter Erstarrung: lokalisierte morphologische Muster

Zusammenfassung

Die fest/flüssig Grenzfläche bei gerichteter Erstarrung tritt in Wechselwirkung mit einer aufgeprägten, stationären, zweidimensionalen Zellularkonvektion. Ist die Wellenlänge der Konvektion $2\pi/\alpha$ deutlich größer als die Wellenlänge $2\pi/\beta$ der morphologischen Instabilität, so erfährt die Grenzfläche eine nahezu parallele Scherung, die durch die vorgegebene Strömung periodisch die Richtung wechselt.

Legt man anstelle der ortsperiodischen zunächst eine konstante Scherströmung zugrunde, so kann mittels einer neuen Formulierung eine ganze Klasse von Scherströmungen einheitlich untersucht werden. Diese Formulierung führt weiterhin zu einem Verständnis der physikalischen Mechanismen.

Für ortsperiodische Scherströmungen können zwei neue Moden einer Instabilität identifiziert werden: Für kleine Werte α/β und bei schwacher Konvektion erweist sich die morphologische Instabilität als nahe den konvergierenden Staupunkten lokalisiert. Die neutralstabile Lösung ist in diesem Fall stationär und in lokalisierten Paketen existieren jeweils viele morphologische Zellen. Für größere Werte α/β oder für stärkere Strömungen hingegen ist die morphologische Instabilität zwischen den Staupunkten lokalisiert. Das instabile Muster der fest/flüssig Grenzfläche wandert innerhalb einer stationären Einhüllenden.

Contents

1	Introduction	3
2	Formulation	7
2.1	Basic equations	7
2.2	Scaled equations	8
2.3	Simplifications	9
2.4	Coordinates	10
3	Morphological instabilities	11
3.1	No buoyancy, no flow	12
3.2	Weak buoyant flow	12
4	Influence of remote flow	17
4.1	The steady basic state	19
4.2	Stability of the basic state	20
4.2.1	Parallel shear flow	20
4.2.2	$\alpha\xi$ -periodic flows	26
5	Numerical solution	31
5.1	Linear stability	32
6	Conclusions	37
7	References	40

1 Introduction

The stability of the solid-liquid phase-transformation interface has for decades been the subject of intense research in crystal growth (see Coriell & McFadden [6]). A stable interface is the key for growing high quality homogeneous single crystals. The complex physics at the interface involves various phenomena such as the liberation of the latent heat of fusion, density changes across the interface, surface-energy effects, conduction of heat in the liquid and solid phase, and convective heat transport in the liquid. Moreover, if the solidifying material consist of a multicomponent material, there may be mass exchange at the interface, diffusive mass transport within the solid and diffusive-convective transport in the liquid. With all these effects the interface becomes an active free boundary governed by a nonlinear coupling between heat, mass and momentum transfer. The position and shape of the interface influence the variables of state at the solidification front and hence determine the microstructure in the crystal.

If the solubility of the second component is smaller in the solid than in the liquid, then there is a rejection of solute at the interface. The flux of rejected solute is removed from the interface by diffusion in the solid and by diffusion and convection in the liquid. A thin concentration layer forms at the interface which is the origin for a morphological instability during solidification. The thickness of this layer is $\delta_c = D/V$, determined by the balance of convective mass flux due to the uniform motion of the material with the pulling speed V and by diffusion in the liquid phase with mass diffusivity D . It is *the* characteristic scale that measures the order of magnitude for the wave length of the growing perturbations. A sketch of the geometry and the main physics is displayed in figure 1.

An analysis of the stability of the planar interface can be found in the classical work of Mullins & Sekerka [16]. The interface remains stable for low pulling speeds. However, once the pulling speed V exceeds a critical value V_c the interface becomes unstable (see figure 2). With increasing pulling speed the concentration layer becomes thinner, the destabilizing concentration gradient stronger. Once the ratio of the concentration gradient to the temperature gradient exceeds a critical value, the instability sets in.

The above described physics is preserved qualitatively if instead of a motionless liquid a weak flow is present in the problem. However, there are some quantitative changes to the stability limits due to the flow. The influences of quite different flows on the stability of a solidification front have been analyzed in the past by a number of authors (see Davis [8]). The influence of buoyancy-driven convective instability competing with morphological instability is discussed e.g. in [4], [12],[13],[18] or in [5]. Unstable (stable) density stratifications are possible due to solutal expansion if the lighter (heavier) component is rejected. The degree of convective destabilization is expressed in terms of a solutal Rayleigh number R . Positive values of R indicate unstable and negative values indicate stable solutal-density stratification. Increasing R from zero, [12],[18] and [5] find a stabilization of the planar interface compared to the pure morphological case when no flow is present. However, if R becomes larger than a critical value, one has to take into account the onset of a convective instability. In the work of [12] the main attention was focused on the case when $R = O(1)$, though one part of the present paper describes situations when buoyant effects are small. This fact allows significant mathematical simplifications of the problem and gives deep insight to the physics. The case

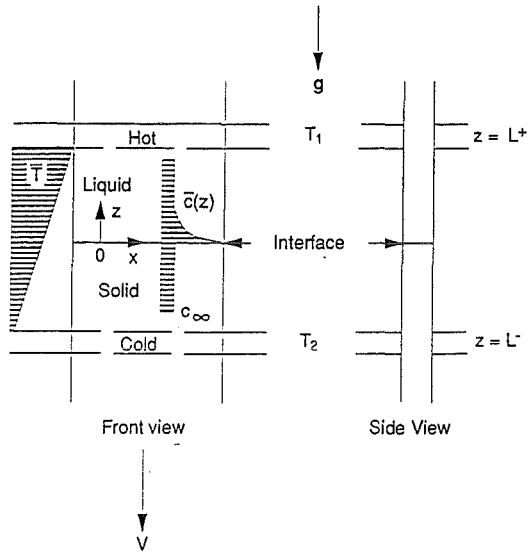


Figure 1: Configuration for directional solidification in a Hele-Shaw cell. The temperature T is linear in the frozen-temperature approximation; $T_1 > T_2$. Solute is rejected at the interface and transferred by diffusion into the liquid. The solute diffusion is negligibly small in the solid phase.

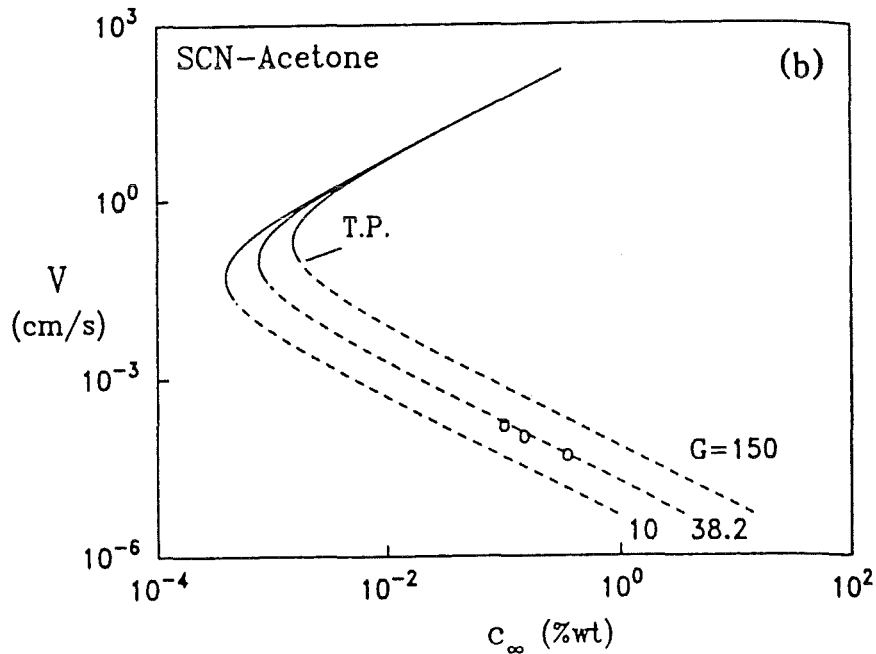


Figure 2: Neutral stability curve of succinotirole-acetone, including the effect of latent heat, at several temperature gradients G [K/cm]. Critical pulling speed versus concentration (taken from [15]). The region inside the curve corresponds to an unstable planar interface.

of weak solutal buoyancy is also presented upon here in order to introduce the reader to the problem of morphological instability influenced by flow. The resulting flow pattern are discussed in detail. It is shown that for long-wave perturbations, the flow above the interface is mainly represented by a locally parallel shear flow exhibiting a viscous layer near the interface within which the uniform velocity of the outer region is matched to the no-slip condition.

Guided by these observations the influence of forced, parallel shear flow on the morphological instability is considered. While in the examples above the flow was driven by the morphological instability itself, now an attempt is made to decouple the physical effect by assuming a remote flow created by some (external) means; the flow is present even if the interface remains planar. Related situations have been considered e.g. by [7] (the plane Couette flow) and [11], [17] (asymptotic suction profile with uniform weak remote flow far from the interface) or originally by [9] (parabolic velocity profile near the interface). The velocity profile used in the present paper is very similar to that used by Forth & Wheeler [10]. Their analytical analysis has been performed for very thick viscous layers. They expand all variables in terms of the Schmidt number Sc which, in their case, determines the thickness of the viscous layer. Results for lower values of Sc could be obtained in their work by numerical solutions. In the present paper it is also assumed that the Schmidt number is large. However, the thickness of the viscous layer is assumed to be governed by other effects and can take any value independently of Sc . As remote flow, a very general family of parallel shear flows is defined here, which covers the Couette flow as well as the asymptotic suction profile with arbitrary boundary layer thickness. It includes the slug flow in the limit of an infinitely thin viscous layer. The obtained results are consistent with those obtained by Forth & Wheeler [10]. A comparison with a solution of [17] shows good agreement as well. By redefining the scaling it is possible to recast all pervious results in a single diagram from which the influence of the viscous-layer becomes clear.

Finally, and most importantly, the stability is analyzed of an interface, above which a pre-existing long-scale spatially-periodic, cellular remote flow is imposed. The flow is chosen similar to that convective flow which establishes at weak buoyancy. The stability of the interface is considered for the case when the wave length $2\pi/\alpha$ of the flow is much larger than the morphological scale $2\pi/\beta$. The case $\alpha \ll \beta$ is considered for instabilities of morphological scale. In this limit the flow along the interface is spatially periodic, the component normal to the interface is negligible and a WKB technique is used to infer the structure of the instability. It is found that the principal instability in this limit has interface deformations exponentially small everywhere except near the converging stagnation points. In neighborhoods of these points there is a *localized* deformation envelope that includes many morphological wave lengths. This work is related to that of Brattkus and Davis [1] who examined plane stagnation-point flow over interfaces.

A direct finite-difference numerical simulation of the linearized problem is then made. A good agreement is found if the product $\alpha\hat{P}$ is sufficiently small. Here \hat{P} is the magnitude of the flow far from the interface.. This restriction is consistent with the analytical solution which requires that $\alpha \rightarrow 0$ and that $\alpha\hat{P} \ll 1$. The numerical and the analytical solution leads to almost the same envelope of localized solutions.

However, if $\alpha\hat{P}$ is not small enough there are even strong qualitative differences be-

tween the numerical predictions and the results obtained analytically assuming $\alpha\hat{P} \ll 1$. The most amplified eigensolution is not located at, but between the stagnation points. The interface exhibits an amplitude modulated wave, travelling with the flow. Infinitesimally small perturbations are amplified along their path from one stagnation point to the other. Along their path, they take largest amplitudes near the location where the velocity has its maximum. Approaching the other stagnation point the envelope decays again to zero. The reason for these two types of solutions will be discussed.

2 Formulation

2.1 Basic equations

Consider the directional solidification of a dilute binary alloy in the given temperature field

$$T = T_0 + Gz \quad (1)$$

where the temperature gradient has only one constant component G in the z -direction. In the Cartesian reference frame (x, y, z) fixed to this temperature field the solidified crystal moves with the constant velocity $-V\hat{\mathbf{z}}$ where V denotes the crystal pulling speed. The Cartesian unit vectors are $\hat{\mathbf{x}}$, $\hat{\mathbf{y}}$, and $\hat{\mathbf{z}}$.

The solid-liquid interface S is located at the position $z = H$, at which the temperature equals the interface temperature T_I according to the *Gibbs-Thomson* relation

$$T_I = T_M + mc - \left(\frac{T_M \gamma}{L_v} \right) K \quad \text{on } S, \quad (2)$$

which assumes *thermodynamic equilibrium*. Here T_I is given by the melting temperature T_M of the pure material changed by the presence of the secondary component with concentration c in the liquid phase. The term mc accounts for constitutional undercooling with m , the slope of the liquidus. The last term gives the capillary undercooling if the liquid interface exhibits a local curvature K . The quantity $T_M \gamma / L_v$ accounts for surface energy effects with the surface energy per area γ and the latent heat of fusion per unit volume L_v . At the interface the concentration in the liquid phase c and in the solid phase c_s are related by

$$c_s = kc \quad \text{on } S. \quad (3)$$

The distribution or *segregation coefficient* k as well as the slope m of the liquidus line can be obtained for thermodynamic equilibrium from the phase diagram of the material.

The *conservation of solute* at the interface requires that

$$v_n(c_s - c) = \mathbf{n} \cdot (D \nabla c) \quad \text{on } S. \quad (4)$$

This condition is already simplified, assuming that the diffusion in the solid crystal is negligibly small and that the density ρ does not change during solidification. The variable v_n denotes the propagation speed of S into the liquid along the unit normal \mathbf{n} and D is the constant solute diffusivity in the liquid phase.

The equations (1-4) relate the concentration at the interface with its location. The concentration in the liquid phase is governed by a convection diffusion equation for the solute

$$\frac{\partial c}{\partial t} + [(\mathbf{v} - V\hat{\mathbf{z}}) \cdot \nabla] c = D \nabla^2 c \quad (5)$$

with equations (1-4) as boundary conditions on S and

$$c = c_\infty, \text{ as } z \rightarrow \infty. \quad (6)$$

Here \mathbf{v} is the deviation of the fluid velocity from the uniform pulling speed.

The flow in the liquid phase is governed by the conservation of mass

$$\nabla \cdot \mathbf{v} = 0 \quad (7)$$

and momentum

$$\frac{\partial \mathbf{v}}{\partial t} + [(\mathbf{v} - V\hat{\mathbf{z}}) \cdot \nabla] \mathbf{v} = -\frac{\nabla p}{\rho} + \nu \nabla^2 \mathbf{v} + \mathbf{f}, \quad (8)$$

where p stands for pressure and \mathbf{f} for a volumetric body force, here given according to the Boussinesq approximation

$$\mathbf{f} = -\rho g \hat{\mathbf{z}} [1 - \alpha_T(T - T_0) - \alpha_s(c - c_0)]. \quad (9)$$

The gravitation vector is $-g\hat{\mathbf{z}}$, the thermal and solutal expansion coefficients are α_T and α_s , respectively. ρ , a reference density, and the kinematic viscosity ν are assumed to be constant. The kinematic boundary conditions are

$$\mathbf{v} = \mathbf{0} \quad \text{on } S \text{ and as } z \rightarrow \infty. \quad (10)$$

2.2 Scaled equations

The governing equations suggest the scales V , D/V^2 , $\delta_c = D/V$, and $\Delta c = (1/k - 1)c_\infty$ for velocity, time, length, and concentration, respectively. Scales for other variables are not explicitly given since they are unimportant for the further analysis. In the following, all variables denote scaled quantities while same symbols are used as for their dimensional counterparts. The non-dimensional variable c stands for the difference of the local concentration and c_∞ , scaled by Δc .

The equations (1- 4) can be combined and give a set of equations relating the concentration c , the propagation speed v_n , and the location of the interface $z = H$.

$$c = 1 - M^{-1}H - \Gamma K \quad \text{on } S. \quad (11)$$

$$v_n [(1 - k)c + k] = \mathbf{n} \cdot \nabla c \quad \text{on } S. \quad (12)$$

Equation (11) gives the thermodynamic equilibrium, and equation (12) describes the conservation of solute. If the analysis were restricted to cases where the deviation of the interface from a planar shape is small, the propagation speed of the interface, its unit normal, and curvature can be approximated by

$$v_n \cong 1 + \frac{\partial H}{\partial t}, \quad \mathbf{n} \cong -(\nabla H) \hat{\mathbf{x}} + \hat{\mathbf{z}}, \quad K \cong -\nabla^2 H. \quad (13)$$

The non-dimensional parameters occurring are the *segregation coefficient* k , the *morphological number*

$$M = m \frac{G_c}{G}, \quad (14)$$

also known as the *Sekerka number*, and the *surface energy parameter*

$$\Gamma = \frac{T_M \gamma}{m G_c \delta_c^2 L_v}. \quad (15)$$

At the solid-liquid interface the morphological number M represents the ratio of temperature variations due to the concentration gradient $G_c = -\Delta c/\delta_c$ and the applied temperature gradient. The liquid is constitutionally undercooled if $M > M_c = 1$ and would then exhibit morphological instabilities if there were no other stabilizing mechanisms. The parameter Γ accounts for capillary undercooling which stabilizes the interface against perturbations with high curvature, i.e. with small wave lengths. Thus, in the presence of surface energy the critical value M_c , at which the first instability is observed, is shifted to values $M_c > 1$.

In non-dimensional notation the equation for concentration in the liquid phase becomes

$$\frac{\partial c}{\partial t} + [(\mathbf{v} - \hat{\mathbf{z}}) \cdot \nabla] c = \nabla^2 c \quad (16)$$

where the boundary condition on S is determined by equation (11) and $c = 0$ as $z \rightarrow \infty$.

The flow in the liquid phase is governed by

$$\frac{1}{Sc} \left[\frac{\partial \mathbf{v}}{\partial t} + [(\mathbf{v} - \hat{\mathbf{z}}) \cdot \nabla] \mathbf{v} \right] = -\nabla p + \nabla^2 \mathbf{v} + \mathbf{f}, \text{ with } \nabla \cdot \mathbf{v} = \mathbf{0} \quad (17)$$

and $\mathbf{v} = \mathbf{0}$ on S and as $z \rightarrow \infty$. The forcing term in the Boussinesq approximation becomes $\mathbf{f} = [R_T T + Rc] \hat{\mathbf{z}}$ if the gravitation vector points opposite to $\hat{\mathbf{z}}$. R_T and R are the thermal and solutal *Rayleigh numbers*

$$R_T = \frac{\alpha_T g G \delta_c^4}{\nu D}, \quad R = \frac{\alpha_s g \Delta c \delta_c^3}{\nu D}, \quad (18)$$

and

$$Sc = \frac{\nu}{D} \quad (19)$$

is the *Schmidt number*.

2.3 Simplifications

For most materials the *Schmidt number* is very large, $Sc \gg 1$, so that the left-hand side of the momentum equation becomes negligible. The physics is still well represented by its simplified version

$$\nabla p = \nabla^2 \mathbf{v} + \mathbf{f}. \quad (20)$$

In the two-dimensional case the velocity field can be expressed as

$$\mathbf{v} = \nabla \times (\psi \hat{\mathbf{y}}), \quad (21)$$

using the scalar stream function ψ , satisfying identically the mass conservation equation for incompressible fluids, $\nabla \cdot \mathbf{v} = \mathbf{0}$. The stream function is determined by

$$\nabla^2 \psi = -\omega, \quad (22)$$

where ω is the (single) y -component of vorticity, $\omega \hat{\mathbf{y}} = \nabla \times \mathbf{v}$. The vorticity ω itself is obtained by taking the curl of the simplified momentum equation (20), using $\nabla \times \mathbf{f} = Rc_x$.

$$\nabla^2 \omega = -Rc_x. \quad (23)$$

Here, and in the following, subscripts like $_{x,z,t}$ denote the corresponding partial derivatives of variables. Due to the *frozen-temperature approximation* [14] there is no contribution of thermal buoyancy in equation (23).

2.4 Coordinates

While above the Cartesian reference frame has been fixed to the frozen temperature field, it is more appropriate to describe the deformation of the solid-liquid interface S in a system fitted to this interface. Therefore, the domain $H \leq z \leq \infty$ is mapped to a finite region $1 \geq \zeta \geq 0$. The new coordinates are

$$\xi = x, \quad \zeta = e^{H-z}, \quad \tau = t. \quad (24)$$

Thus, $z = \infty$ becomes $\zeta = 0$.

With these coordinates the governing equations read

$$\mathbb{L}\omega = -R(c_\xi + \zeta H_\xi c_\zeta), \quad (25)$$

$$\mathbb{L}\psi = -\omega, \quad (26)$$

$$c_\tau + \zeta(\psi_\zeta c_\xi + [1 - \psi_\xi + H_\tau] c_\zeta) = \mathbb{L}c \quad (27)$$

where \mathbb{L} denotes the *Laplacian* in the new coordinates,

$$\nabla^2 \rightarrow \mathbb{L} = \partial_{\xi\xi} + (1 + H_\xi^2)(\zeta^2 \partial_{\zeta\zeta} + \zeta \partial_\zeta) + 2\zeta H_\xi \partial_{\xi\zeta} + \zeta H_{\xi\xi} \partial_\zeta. \quad (28)$$

The equilibrium condition and the conservation of solute at the interface $\zeta = 1$ are

$$c = 1 - M^{-1}H + \Gamma H_{\xi\xi}, \quad (29)$$

$$(1 + H_\tau)([1 - k]c + k) = H_\xi c_\xi + (1 + H_\xi^2) c_\zeta. \quad (30)$$

3 Morphological instabilities

Consider the stability of the planar interface against infinitesimally small perturbations and focus attention to the fastest growing eigenmode of the interface deformation $H = H_0 + \varepsilon H_1 e^{i\alpha\xi + \sigma\tau}$ by expanding all variables in terms of the small parameter ε

$$\begin{pmatrix} \omega \\ \psi \\ c \end{pmatrix} = \begin{pmatrix} \omega_0(\zeta) \\ \psi_0(\zeta) \\ c_0(\zeta) \end{pmatrix} + \varepsilon \begin{pmatrix} \omega_1(\zeta) \\ \psi_1(\zeta) \\ c_1(\zeta) \end{pmatrix} e^{i\alpha\xi + \sigma\tau} + \dots \quad (31)$$

H_1 might be set to 1, but it is kept arbitrary here for convenience. In the proceeding chapters, when the wave length of the flow and the wave length of the morphology differ essentially, H_1 may vary on the long scale of the flow. Assume disturbances to be periodic in ξ with real wave number α and complex growth rate σ . After collecting equal powers in ε one finds at $O(1)$:

$$\zeta^2 \omega_{0\zeta\zeta} + \zeta \omega_{0\zeta} = 0, \quad (32)$$

$$\zeta^2 \psi_{0\zeta\zeta} + \zeta \psi_{0\zeta} = -\omega_0, \quad (33)$$

$$\zeta^2 c_{0\zeta\zeta} = 0. \quad (34)$$

The solutions in this order, which vanish at infinity, $\zeta \rightarrow 0$, and which satisfy the interface conditions $\psi_0 = \psi_{0\zeta} = 0$, $c_0 = 1 - M^{-1}H_0$, $c_0(1 - k) + k = c_{0\zeta}$ at $\zeta = 1$ are:

$$H_0 = \omega_0 = \psi_0 = 0, \quad c_0 = \zeta. \quad (35)$$

In the order $O(\varepsilon)$ the equations for the perturbations read

$$\zeta^2 \omega_{1\zeta\zeta} + \zeta \omega_{1\zeta} - \alpha^2 \omega_1 = -i\alpha R (c_1 + \zeta H_1), \quad (36)$$

$$\zeta^2 \psi_{1\zeta\zeta} + \zeta \psi_{1\zeta} - \alpha^2 \psi_1 = -\omega_1, \quad (37)$$

$$\zeta^2 c_{1\zeta\zeta} - (\alpha^2 + \sigma) c_1 = \zeta [(\alpha^2 + \sigma) H_1 - i\alpha \psi_1] \quad (38)$$

with vanishing values of ω_1, ψ_1 , and c_1 at $\zeta = 0$ and interface conditions $\psi_1 = \psi_{1\zeta} = 0$, $c_1 = -(M^{-1} + \Gamma\alpha^2)H_1$, $\sigma H_1 + c_1(1 - k) = c_{1\zeta}$ at $\zeta = 1$.

A solution to this problem can be obtained by eliminating successively all variables and solving a sixth order ODE for ψ_1 . If one were mainly interested in the influence of a weak flow, induced by solutal buoyancy, $\alpha R \ll 1$, it would be easier to expand the variables in powers of αR .

$$\begin{pmatrix} \omega_1 \\ \psi_1 \\ c_1 \end{pmatrix} = \begin{pmatrix} \omega_{10} \\ \psi_{10} \\ c_{10} \end{pmatrix} + \alpha R \begin{pmatrix} \omega_{11} \\ \psi_{11} \\ c_{11} \end{pmatrix} + \dots \quad (39)$$

as well as the control parameter and growth rate

$$M^{-1} = 1 - \alpha^2 \Gamma + g_0 + \alpha R g_1 + \dots \quad (40)$$

$$\sigma = \sigma_0 + \alpha R \sigma_1 + \dots \quad (41)$$

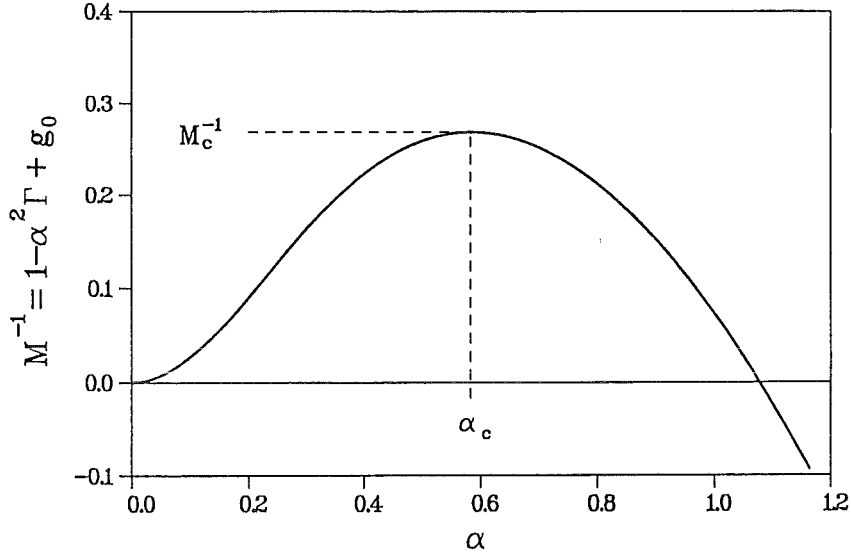


Figure 3: Marginal stability of a planar interface without flow. M^{-1} versus α for $k = 0.3$ and $\Gamma = 0.6$.

3.1 No buoyancy, no flow

In the order $\varepsilon(\alpha R)^0$ the solution for marginal stability, $\sigma_0 = 0$, is equivalent to results obtained by Mullins & Sekerka [16]. $\omega_{10} = \psi_{10} = 0$ and

$$c_{10} = -H_1 (\zeta + g_0 \zeta^\mu) \quad (42)$$

with

$$g_0 = \frac{k}{1 - k - \mu}, \quad (43)$$

where the solution contains the value H_1 , the $O(1)$ initial value of the interface deformation. The abbreviation $\mu = \frac{1}{2} + \frac{1}{2}\sqrt{1 + 4\alpha^2}$ is introduced here for convenience.

Figure 3 shows results for the marginal stability, $\sigma_0 = 0$, (it is known that σ_0 is real) for the case of zero gravity, $R = 0$. The control parameter is M^{-1} . The results shown in this figure are obtained for a lead-tin alloy using $k = 0.3$, and $\Gamma = 0.6$ to show the agreement with previous calculation, for example shown in [17]. The planar interface is stable against perturbations with any wave number for parameters above the curve and unstable for those below. A first instability occurs if $M^{-1} = M_c^{-1} = 0.2679$ with the critical wave number $\alpha_c = 0.5818$. For $M^{-1} < M_c^{-1}$ there exists a band of unstable wave numbers.

3.2 Weak buoyant flow

The influence of a weak buoyant flow is reflected by the solution at the order $\varepsilon(\alpha R)^1$. At this approximation the equations read:

$$\zeta^2 \omega_{11\zeta\zeta} + \zeta \omega_{11\zeta} - \alpha^2 \omega_{11} = i g_0 H_1 \zeta^\mu, \quad (44)$$

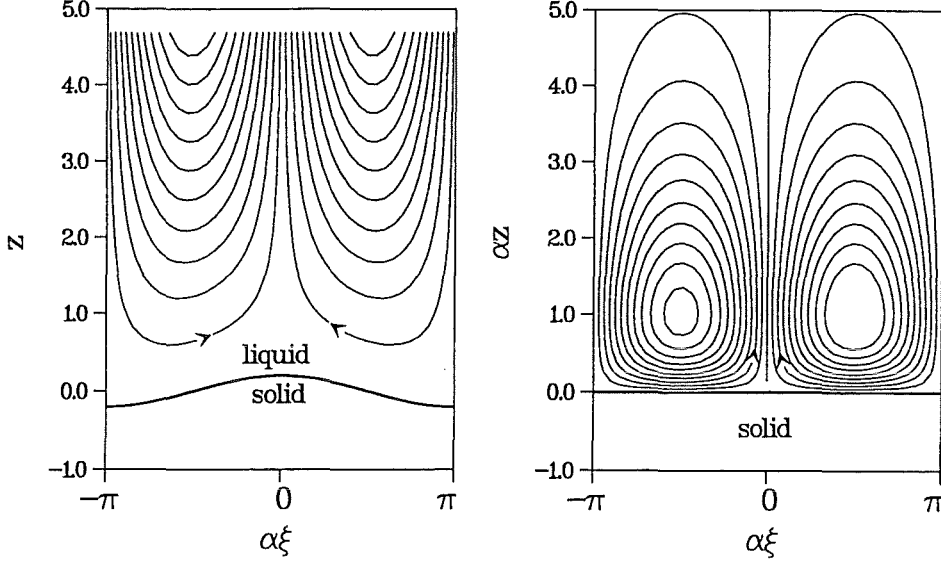


Figure 4: Streamlines above a perturbed interface for $\alpha \ll 1$ in the near field (a) and in the far field (b). The indicated flow direction holds for $R > 0$. For $R < 0$ the flow would be reversed.

$$\zeta^2 \psi_{11\zeta\zeta} + \zeta \psi_{11\zeta} - \alpha^2 \psi_{11} = -\omega_{11}, \quad (45)$$

$$\zeta^2 c_{11\zeta\zeta} - \alpha^2 c_{11} = -(\sigma_1 g_0 H_1 \zeta^\mu + i\alpha \psi_{11\zeta}) \quad (46)$$

with vanishing values of unknowns at $\zeta = 0$ and $\psi_{11} = \psi_{11\zeta} = 0$, $\sigma_1 H_1 + c_{11}(1-k) = c_{11\zeta}$ at $\zeta = 1$. A straight-forward integration leads to the solution

$$\psi_{11} = i \frac{g_0 H_1}{(\alpha^2 - \mu^2)^2} \{ [(\alpha - \mu) \ln \zeta - 1] \zeta^\alpha + \zeta^\mu \}. \quad (47)$$

This solution is now discussed in some detail. The flow exhibits two distinct scales in z , associated with two different physical mechanisms. The first one is the balance between the driving buoyant force and the dissipation in the viscous layer near the interface. The characteristic length scale here is $1/\mu$. The other one is the viscous dissipation in the far field with its scale $1/\alpha$. For $\alpha \ll 1$ the two scales disparate. Viscous effects in the far field become very weak so that large distances are necessary on which the fluid slows down as $\alpha z \gg 1$. More important are viscous effect near the interface. Notice that $\mu \rightarrow 1$ as $\alpha \rightarrow 0$. The fluid velocity is zero at the interface and reaches its maximum value as $\mu z = z \gg 1$. In figure 4, the streamlines in the near field and in the far field are displayed. The associated velocity component tangential to the interface is displayed in the figures 5 for the near field and for the far field. To quantify the results the following coordinates are introduced: the coordinate on the morphological scale with its origin on H is denoted by $z' = z - H$, while the coordinate on the large scale is written as $Z = \alpha(z - H)$. With these scales and coordinates the streamfunction (47) becomes

$$\psi = \varepsilon P(\alpha \xi) \left[(1 + Z - z') e^{-Z} - e^{-z'} \right] + O(\varepsilon^2). \quad (48)$$

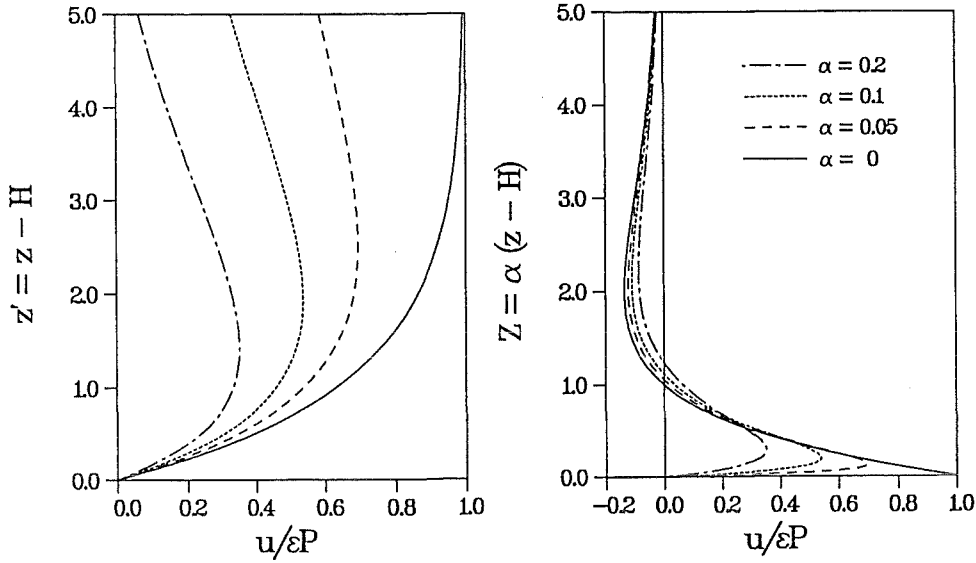


Figure 5: Tangential velocity of a flow above a perturbed interface for various values of α . a) in the near field, b) in the far field.

The strength of the flow is expressed by ε times $P(\alpha\xi)$, where

$$P(\alpha\xi) = \frac{\alpha H_1 R g_0}{(\alpha^2 + \mu^2)^2} e^{i\alpha\xi}. \quad (49)$$

Note, $\varepsilon\alpha H_1$ is proportional to the slope of the initial small perturbation of the planar interface. The intensity of the flow is proportional to this value and scales in addition with Rg_0 . For $\alpha \rightarrow 0$ the denominator becomes unity and the product Rg_0 corresponds to a solutal Rayleigh number in which the characteristic concentration difference Δc is simply given by c_∞ as $k \ll 1$.

The resulting velocity components are up to the leading order:

$$u = -\psi_z = \varepsilon P(\alpha\xi) \left[(1 - Z) e^{-Z} - e^{-z'} \right] \quad (50)$$

and

$$w = \psi_x = \varepsilon P'(\alpha\xi) \alpha \left[(1 + Z - z') e^{-Z} - e^{-z'} \right]. \quad (51)$$

The flow is characterized by an *exponential* viscous layer near the interface, in which the tangential velocity increases from zero to $\varepsilon P(\alpha\xi)$. The flow is driven by solutal convection, with contributing force terms only within the concentration layer. This results in a thickness of this layer of order unity. Since the far field is motionless, all variables must decay to zero as z , or more precisely, as Z tends to infinity. For cases with $\alpha \ll 1$, this decay is very slow. Important for the morphology is the solution near the interface, i.e. as $Z \rightarrow 0$. Near the interface the significant part of the flow is simply given by its tangential component $u \sim 1 - e^{-z'}$. The flow varies with ξ according to the

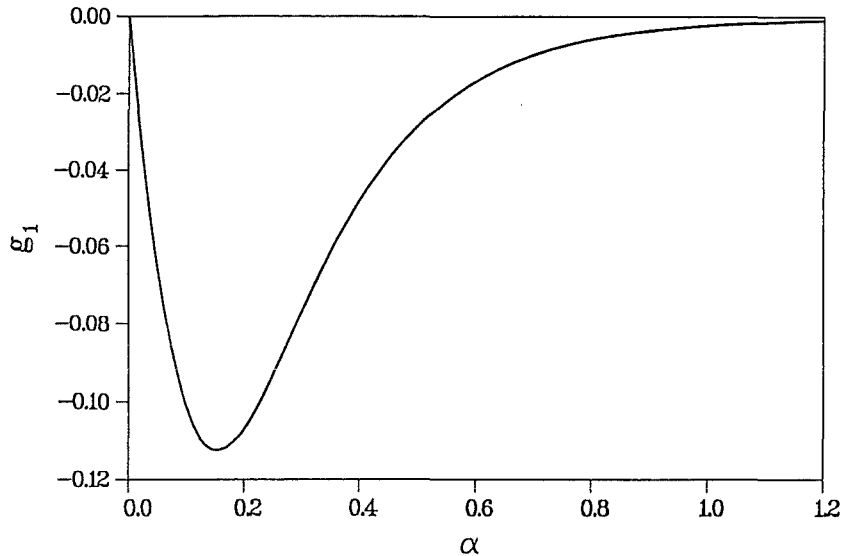


Figure 6: Correction g_1 to the stability threshold due to a weak, buoyancy-induced flow versus α for $k = 0.3$

harmonic function $P(\alpha\xi)$. The component of velocity normal to the interface is smaller by an order of α .

If $\xi = 0$ is chosen at a stagnation point, one recovers for small z' , $u \sim \xi z'$ and $w \sim -\alpha z'^2$, previously used as given velocity profile in stability considerations by Brattkus & Davis [1]. The analysis in [1] focuses on long-wave instabilities where $\partial/\partial\xi \sim \alpha$ with $\alpha \ll 1$. Therefore, $u\partial/\partial\xi$ and $w\partial/\partial z'$ are both of the same order of magnitude and are treated simultaneously in their analysis. In contrast, the present analysis does not use a long-wave approximation. Perturbations are allowed to take any wave number ($\gg \alpha$), even values of $O(1)$ or larger. The normal-to-the-interface component of velocity w does not affect the stability at leading order in α whereas in the analysis of Brattkus & Davis this velocity component was very important. Thus, in the present problem at leading order, here the problem reduces to that of a parallel shear flow with ξ -periodic magnitude above an interface.

The integration of the concentration equation leads to a lengthy expression for c_{11} , not displayed here. Finally the condition $c_{11} = -H_1 g_1$ at $\zeta = 1$ determines the correction to the pure morphological case [16] due to weak solutal convection,

$$g_1 = -\frac{\alpha k}{2\mu(\mu - 1 + k)^2(\mu + \alpha)^4}. \quad (52)$$

These results are displayed in figure 6. Since $g_1 < 0$, the solutal buoyancy is stabilizing for $R > 0$, which corresponds to the case when the density ρ of the fluid decreases with increasing c . For $R < 0$ the buoyancy destabilizes the planar interface.

These results can be interpreted as follows: Above a perturbed interface the fluid has a negative concentration gradient $c_z < 0$. This concentration gradient is the driving mechanism for morphological instabilities. For $R > 0$ the related density gradient is $\rho_z > 0$, which leads to an unstable stratification with lighter fluid near the interface and

heavier fluid above in the far field. This induces a flow "uphill", with stagnation points near the crests and troughs (see e.g. figure 4). At the troughs the flow points away from the interface, reducing the magnitude of c_z and thus slowing down the propagation of the interface. Near the crests the flow points towards the interface, increasing the absolute value of c_z and the interface speed. This leads to a stabilization of an initially disturbed planar interface. The above results are in accordance with results obtained in [18] if $R < R_c$, the critical value for the onset of solutal buoyant instabilities called convective instabilities. For $R > R_c$ convective instabilities lead to a formation of flow patterns even above a flat interface.

For $R < 0$ the opposite holds. The fluid has a stable density stratification. There are no convective instabilities to be expected in this range of parameters. Nevertheless, it is remarkable, that gravity now tends to destabilize the interface [5].

4 Influence of remote flow

In the previous section the pure morphological stability problem has been considered as well as the case of weak buoyant flow, induced by solutal convection at a deformed interface. Common for both situations is the fact that there is no flow if the interface remains planar i.e. if the solidification front is stable. Here, the influence of a remote flow on the morphological stability is studied. Cases with flow are considered, even if the interface remains stable. Such flows are independent of ε , the small parameter which is still used to describe the deviations from the stationary interface.

$$H = H_0 + \varepsilon H_1 e^{i\beta\xi + \sigma\tau}. \quad (53)$$

Here and in the rest of the paper, one distinguishes between the scale of the flow, the wave number of which is called α and the wave number β of the interface perturbations due to morphological instability. As given remote flows, the representation of the stream function is used, similar to that in the previous chapter and attention is restricted to the region near the interface.

$$\psi_0 = P(\alpha\xi) \left[(s - z') - s e^{-z'/s} \right]. \quad (54)$$

The flow may still depend on $\alpha\xi$ with $\alpha \ll 1$. Moreover, assume that the variation with ξ of the flow ψ_0 is independent of variations due to morphological changes and happens on much longer scales, $\alpha \ll \beta$. The parameter s distinguishes members of a general class of flows. It represents the thickness of the viscous layer near the interface, in which the tangential velocity u_0 decays from the value $P(\alpha\xi)$ to zero at $z' = 0$.

$$u_0 = -\psi_{0z} = P(\alpha\xi) \left[1 - e^{-z'/s} \right]. \quad (55)$$

Such flows exist in crystal growth applications. The case of an asymptotic suction profile, where P is constant in ξ , has been considered in the past by several authors (see e.g. [10], [17], [11], or [9] who used the first two terms in a power series expansion of equation (55)). The asymptotic suction profile is an exact solution of the momentum equation for a translational motion of the crystal, when the condition far from the interface becomes $u = P$ as $z' \rightarrow \infty$. The parameter s is then equivalent to the *Schmidt number* Sc .

In the present analysis it is assumed that the Schmidt number is very large, while the thickness of the viscous layer can take any value $s > 0$. Flows with $s = 1$ are possible due to solutal convection in an imperfect experimental apparatus, if the pulling direction (direction of the temperature gradient) does not coincide exactly with the direction of the gravitation vector. In this case the magnitude of the flow is proportional to the solutal *Rayleigh number* R and the deviation from a perfect alignment. Boundary layers of exponential type are also known for electrically conducting fluids within strong magnetic fields. For such applications the boundary-layer thickness may take any desired value according to the strength of the applied magnetic field and s becomes a new additional control parameter.

In addition to these unidirectional flows, flows with periodic variations $P(\alpha\xi) = iPe^{i\alpha\xi}$ emerge from the imposition of the long-scale cellular convection on the interface

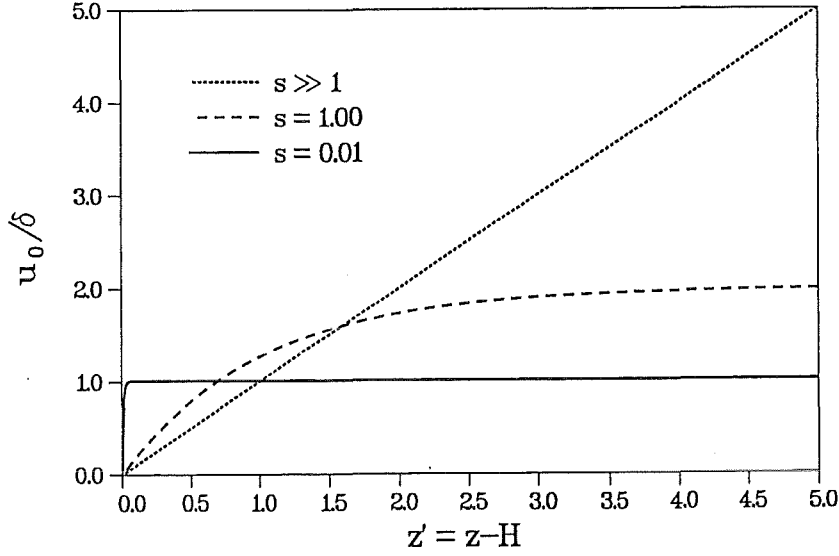


Figure 7: Remote flow: Tangential velocity component u_0 near the interface for various values of s . The scale $\delta = P/(1+s)$ has been introduced for convenience.

as discussed earlier. A remote flow depending on αx may be caused e.g. by a weakly inhomogeneous temperature field, if there are small lateral heat losses. Then, $P(\alpha\xi)$ can be considered as a Fourier component of such flows.

The fact that the morphological scale and the scale of the flow differ strongly suggest the use of multiple scales:

$$\eta = \alpha\xi, \quad \eta_m = \beta\xi, \quad (56)$$

where η is the coordinate on the scale of the flow (the slow ξ) and η_m stands for the morphological coordinate (the fast ξ). Derivatives transform as follows:

$$\partial_\xi \rightarrow \alpha\partial_\eta + \beta\partial_{\eta_m}.$$

In the coordinates introduced earlier, the stream function of the remote flow reads

$$\psi_0 = iP(\eta) [s + \ln \zeta - s\zeta^{1/s}]. \quad (57)$$

In general, the stationary basic solution H_0 , the stability of which is the subject of further investigations, is no longer uniform in η if the flow varies with η . The deformation of the interface is now expressed as

$$H = H_0(\eta) + \varepsilon H_1(\eta, \eta_m) e^{\sigma\tau} \quad (58)$$

and the other variables are expanded in powers of the small parameter ε .

$$\begin{pmatrix} \omega \\ \psi \\ c \end{pmatrix} = \begin{pmatrix} \omega_0(\eta, \zeta) \\ \psi_0(\eta, \zeta) \\ c_0(\eta, \zeta) \end{pmatrix} + \varepsilon \begin{pmatrix} \omega_1(\eta, \eta_m, \zeta) \\ \psi_1(\eta, \eta_m, \zeta) \\ c_1(\eta, \eta_m, \zeta) \end{pmatrix} e^{\sigma\tau} + \dots \quad (59)$$

4.1 The steady basic state

The stationary solution is determined from the expanded equations with $\varepsilon = 0$. For values $\alpha \ll 1$ assume the given flow according to equation(57) and expand all variables in powers of the other small parameter $\alpha P/(1+s)$.

$$\begin{pmatrix} H_0(\eta) \\ c_0(\eta, \zeta) \end{pmatrix} = \begin{pmatrix} H_{00} \\ c_{00}(\zeta) \end{pmatrix} + \frac{\alpha P(\eta)}{(1+s)} \begin{pmatrix} H_{01}(\eta) \\ c_{01}(\eta, \zeta) \end{pmatrix} + \dots \quad (60)$$

For a common presentation of results over a whole range of the parameter $0 \leq s \leq \infty$ it will turn out that this expansion parameter is very convenient. With this notation the $O(1)$ parameter $\delta = P/(1+s)$ represents the magnitude of the velocity near the interface for $s \ll 1$ and the velocity gradient for $s \gg 1$. This scale is introduced here, since only the magnitude of the flow is important when the concentration field is subjected to a flow with an extremely thin viscous layer, while for very thick viscous layers the velocity gradient is the characteristic measure for convective transport phenomena.

If this expansion is used in the basic equations (27-30) one finds at $O(\varepsilon^0, (\alpha\delta)^0)$,

$$\zeta^2 c_{00\zeta\zeta} = 0 \quad (61)$$

with vanishing values at infinity, as $\zeta = 0$, and interface conditions $c_{00} = 1 - M^{-1}H_{00}$, $c_{00}(1-k) + k = c_{00\zeta}$ at $\zeta = 1$. The equation and the boundary conditions hold for the case with no flow and have been discussed already in section 3 dealing with the pure morphological instability. The solution in this order of approximation is

$$H_{00} = 0, c_{00} = \zeta. \quad (62)$$

The equation for c_{01} and the interface conditions in the order (αP) read:

$$\zeta^2 c_{01\zeta\zeta} = \zeta (\psi_{0\zeta} c_{00\eta} - i\psi_0 c_{00\zeta}), \quad (63)$$

$$c_{01} = -M^{-1}H_{01}, \quad (64)$$

$$c_{01}(1-k) = c_{01\zeta}. \quad (65)$$

The integration of this set of equations leads to the solution

$$c_{01} = \zeta \left(\frac{1}{k} + (s^2 - 1) \ln \zeta + \frac{1}{2} (s+1) \ln^2 \zeta + s^3 (1 - \zeta^{1/s}) \right). \quad (66)$$

Results are shown in figure 8 for $s = 0, 1, \infty$. Here, for simplicity, the limit for $s \rightarrow 0$ is displayed in equation (67). The solution for $s \rightarrow \infty$ deviates from the latter one only by $-\frac{1}{6}\zeta \ln^3 \zeta$.

$$H_{01} = -\frac{1}{kM^{-1}}, \text{ and } c_{01} = \zeta \left(\frac{1}{k} - \ln \zeta + \frac{1}{2} \ln^2 \zeta \right) \text{ as } s \rightarrow 0. \quad (67)$$

Near the interface as $\zeta \rightarrow 1$ all solutions coincide and asymptote to $c_{01} \rightarrow 1 + (\frac{1}{k} - 1) \zeta$.

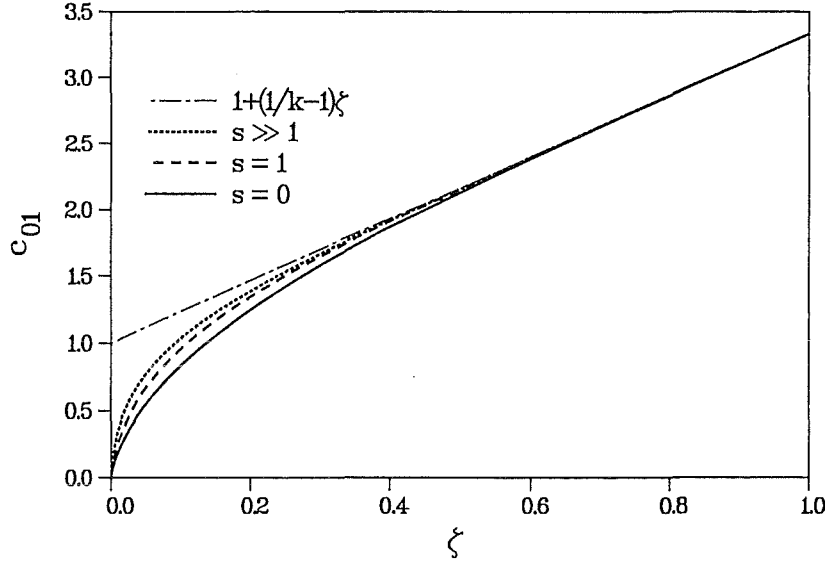


Figure 8: Remote flow: Stationary solution for the concentration c_{01} versus the coordinate ζ for $k = 0.3$ and various values of s . The solution near the interface $\zeta = 1$ asymptotes to $c_{01} = 1 + (\frac{1}{k} - 1)\zeta$ for all s .

4.2 Stability of the basic state

4.2.1 Parallel shear flow

The stability of the basic state is determined by the solution of the equations at order ε . The variables according to the ansatz (59) are written in normal modes

$$(H_1, \omega_1, \psi_1, c_1) \rightarrow (H_1, \omega_1, \psi_1, c_1) e^{i\eta m}. \quad (68)$$

In the limit of $\alpha \rightarrow 0$ the problem reduces to that of a locally parallel shear flow. In this limit, the magnitude of the flow P is constant in ζ . Neglect body forces, and find at $O(\varepsilon)$ the equations

$$\zeta^2 \omega_{1\zeta\zeta} + \zeta \omega_{1\zeta} - \beta^2 \omega_1 = -H_1 \beta^2 (\zeta^3 \psi_{0\zeta\zeta\zeta} + 3\zeta^2 \psi_{0\zeta\zeta} + \zeta \psi_{0\zeta}), \quad (69)$$

$$\zeta^2 \psi_{1\zeta\zeta} + \zeta \psi_{1\zeta} - \beta^2 \psi_1 = H_1 \beta^2 \zeta \psi_{0\zeta} - \omega_1, \quad (70)$$

$$\zeta^2 c_{1\zeta\zeta} - (\beta^2 + \sigma + i\beta\zeta\psi_{0\zeta}) c_1 = H_1 \zeta (\beta^2 + \sigma) + i\beta\zeta\psi_1 \equiv H_1 r \quad (71)$$

with the restriction that the variables must remain finite at infinity, as $\zeta \rightarrow 0$ and with the interface conditions

$$\left. \begin{aligned} \psi_1 &= \psi_{1\zeta} = 0, \\ c_1 &= -H_1 (M^{-1} + \Gamma\beta^2), \\ c_1(1-k) - c_{1\zeta} &= -H_1\sigma. \end{aligned} \right\} \text{ at } \zeta = 1. \quad (72)$$

The right-hand sides of these equations are functions in ζ , known from the solution in the first order as $\varepsilon \rightarrow 0$ and by successive solution of this set of equations. They are proportional to H_1 , which describes the deviations from the stationary interface position

at this order of approximation. Our task is to integrate the set of ordinary differential equations along ζ . The integration constants are expressed as multiples of H_1 . The value H_1 remains unknown and is to be determined later. Note, that the equations do not contain any dependence on the morphological coordinate η_m . Variations of unknowns with this coordinate have been taken into account by introducing normal modes $\sim e^{i\eta_m}$. Their influence on the solution is still present and enters the problem in form of the parameter β in the equations above.

A solution to the vorticity equation is:

$$\omega_1 = i \frac{PH_1}{(b^2 - s^2)} (\zeta^{1/s} + a\zeta^{1/b}), \quad (73)$$

where a is an integration constant to be determined later. Instead of the morphological wave number β , here $b = 1/\beta$ is used for convenience. In this notation, s and b represent characteristic dimensions of the flow and the small-scale morphology, respectively. Given ω_1 , solutions for the streamfunction ψ_1 can be obtained.

$$\psi_1 = i \frac{PH_1}{(b^2 - s^2)^2} \left\{ [b^4 - (s^3 - 2sb^2 + b^3) \ln \zeta] \zeta^{1/b} + s^2 [s^2 - 2b^2] \zeta^{1/s} + (b^2 - s^2)^2 \right\}. \quad (74)$$

This representation allows the existence of a non-uniformity in the solution as $b \rightarrow s$. Fortunately this non-uniformity is not present.

$$\psi_1 = iPH_1 \left\{ \left(1 - \frac{1}{s} \ln \zeta - \frac{1}{8s^2} \ln^2 \zeta \right) \zeta^{1/s} - 1 \right\} \text{ as } b \rightarrow s. \quad (75)$$

Therefore, the equation (74) is uniformly valid over the whole range of wave numbers.

The solution of the concentration equation (71) is obtained using the *method of variation of parameters*. With equation (57), the two solutions to the homogeneous equation

$$\zeta^2 c_{h\zeta} - [\beta^2 + \sigma + -\beta P (1 - \zeta^{1/s})] c_h = 0 \quad (76)$$

are the *Bessel functions* of the first and second kind

$$c_{h1} = \sqrt{\zeta} J_n \left(2s \sqrt{-\beta P} \zeta^{\frac{1}{2s}} \right), \quad (77)$$

$$c_{h2} = \sqrt{\zeta} Y_n \left(2s \sqrt{-\beta P} \zeta^{\frac{1}{2s}} \right), \quad (78)$$

of the order $n = 2s \sqrt{\frac{1}{4} + \sigma + \beta^2 - \beta P}$. For the further analysis, however, it is more convenient to use their representation in form of generalized power series. They can be obtained from the solutions above using mathematical handbooks or directly using *Frobenius* method by substituting a solution of the form

$$c_{h1,2} = \sum_{\nu=0}^{\infty} C_{\nu} \zeta^{\mu_{1,2} + \nu/s} \quad (79)$$

into the homogeneous equation. After collecting corresponding powers one can obtain from the lowest power in ζ the condition

$$\mu_{1,2}^2 - \mu_{1,2} - \sigma - \beta^2 + \beta P = 0, \quad (80)$$

determining the values of

$$\mu_{1,2} = \frac{1}{2} (1 \pm W) \quad (81)$$

where $W = -\sqrt{1 + 4(\sigma + \beta^2 - \beta P)}$ is the Wronskian of c_{h1} and c_{h2} . The successive determination of the coefficients in the expansion (79) finally results in

$$c_{h1,2} = \sum_{\nu=0}^{\infty} \frac{(i\beta P s^2)^\nu}{\nu! \prod_{j=1}^{\nu} (j \mp sW)} \zeta^{\frac{1}{2} \mp \frac{W}{2} + \frac{\nu}{s}}. \quad (82)$$

A particular solution to equation (71) is found as

$$c_p = H_1 \left(c_{h2} \int \frac{c_{h1} r}{W} d\zeta - c_{h1} \int \frac{c_{h2} r}{W} d\zeta \right). \quad (83)$$

The evaluation of c_p is performed using truncated series. The final results are obtained with $\nu_{max} = 10$. Checks with $\nu_{max} = 12$ confirm the quality of the approximation.

The solution for the concentration field is obtained as

$$c_1 = A c_{h1} + H_1(\dots). \quad (84)$$

The unknown coefficient A multiplies the homogeneous solution c_{h1} . The second homogeneous solution does not appear due to vanishing values at $\zeta = 0$. The lengthy formula for c_1 is not shown here, but the main ideas of the solution for the stability problem are resumed.

After having obtained the solution in the form (84) it can be used in the equations for the interface conditions (72). This leads to a 2×2 homogeneous linear system for the unknowns A and H_1 .

$$\begin{pmatrix} b_{11} & b_{12} \\ b_{21} & b_{22} \end{pmatrix} \begin{pmatrix} A \\ H_1 \end{pmatrix} = \begin{pmatrix} 0 \\ 0 \end{pmatrix}. \quad (85)$$

The solution to the stability problem is obtained by the fact, that the determinant of this system must vanish for non-trivial solutions.

$$\det \begin{pmatrix} b_{11} & b_{12} \\ b_{21} & b_{22} \end{pmatrix} = 0. \quad (86)$$

At the limit of stability $\sigma_r = 0$, there remain the two unknowns: σ_i , the frequency of oscillations and g , the control parameter which can be determined from the condition that the real part and the imaginary part of the determinant have to vanish simultaneously. Values for σ_i and g are obtained by *Newton's method* for the roots of nonlinear systems. This procedure can directly be applied for a pure parallel shear flow, if $P = const$, i.e. for asymptotic suction profiles.

All calculations have been performed using the symbolic algebra package *MAPLE*. The formulas for matrix entries are translated into Fortran code. The values for σ_i and g are evaluated with the Fortran program.

In this paragraph the results are described for the case of a remote flow given as parallel shear flow according to a generalized asymptotic suction profile. Using the theory described above the solution for the concentration has been expanded in a generalized power series up to the order $\nu_{max} = 10$. The resulting eigenvalue problem (86) is solved by Newton's method for the values of the control parameter g ($M^{-1} = 1 - \beta^2 \Gamma + g$) and the imaginary part of the growth rate σ_i at marginal stability $\sigma_r = 0$. Results for weak remote flows with $\delta = P/(1+s) \ll 1$ are shown first. Since changes in the morphological stability are expected to be small compared to the case with no flow ($\sigma_{0i} = 0$, g_0 , see previous chapters), the results are displayed in terms of small corrections (σ_{1i} , g_2) to these predictions. The corrections are defined as

$$g = g_0 + \delta^2 g_2, \quad (87)$$

$$\sigma = \delta \sigma_1. \quad (88)$$

These definitions are motivated by the fact that the stability condition given by the critical value of the control parameter should be invariant with the direction of the flow. The correction appears here for the first time in the order δ^2 . However, the direction along which waves may travel induced by the flow should depend on the flow direction. The correction to σ appears therefore in the first order $\sigma = \delta \sigma_{1i}$ and is proportional to $(-\beta)$ times the phase velocity. For cases with $\sigma_{1i} < 0$ the waves travel with the flow, while for $\sigma_{1i} > 0$ the waves travel against the remote flow direction. The arguments for a scaling with $(1+s)$ have been already given in the chapter dealing with the basic steady state solution. Moreover, it will turn out that with this scale the corrections g_2 and σ_1 are near unity. This fact clearly demonstrates that the scale chosen here is the appropriate one for parallel shear flows with very thick viscous layers. The morphology is influenced by properties within the concentration layer. A characteristic measure of the flow near the interface can not be the velocity at infinity as used e.g. by [17], but the velocity gradient at the interface. The results that are displayed in the paper [17] using their scale are near 10^{-5} . Despite the different scaling it can be shown that for the value of $s = 81$ the results coincide with numerical accuracy.

In figure 9 g_2 is plotted versus β for various values of s . For small values of s , when the concentration field is subjected mainly to a uniform flow, the correction to the control parameter is negative over the whole range of β considered. Therefore, the flow stabilizes the steady basic solution. The smallest value of s for which results are displayed is $s = 0.01$. Results for smaller values do almost not differ from this curve.

For larger values of s there exists a band of wave numbers $0 \leq \beta \leq \beta_g^*(s)$ in which the flow destabilizes the basic state. One can find a limiting value $s^* = 1.305$ for which $\beta_g^*(s^*) = 0$. For $s < s^*$ the flow never destabilizes the stationary interface. The highest value for which results are shown is $s = 1000$. Curves for smaller values $1 \ll s < 1000$ are quite similar to this one. Results for large s differ only when β is small, when the morphological wave length becomes comparable to the viscous layer thickness, $b = 1/\beta \sim s$. For very small values of β one can conclude that with increasing s the interface becomes more and more unstable.

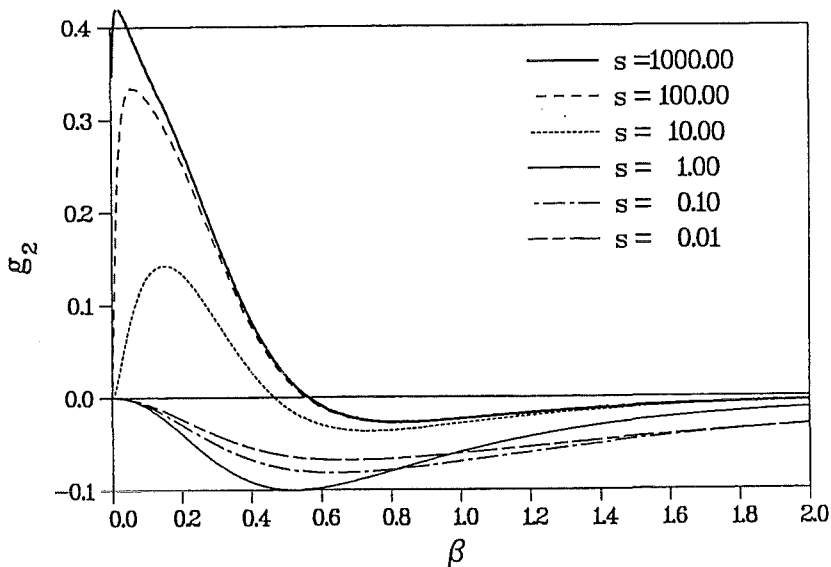


Figure 9: Correction g_2 due to a weak remote parallel shear flow to the stability results without flow versus the morphological wave number β for different values of s . The flow stabilizes the stationary interface for $s < 1.305$. For larger s there exists a band of destabilized wave numbers.

Figure 10 displays results for σ_{1i} versus β . For all values in the range $0 < s < s^*$ the perturbations are travelling waves which move against the direction of the flow. For $s > s^*$ there exists a band of wave numbers $0 \leq \beta \leq \beta_g^*(s)$ within which the waves travel with the imposed fluid flow. Note, however, $\beta_g^*(s) \neq \beta_\sigma^*(s)$.

The functions $\beta_g^*(s)$ and $\beta_\sigma^*(s)$ are shown in figure 11. It can be seen that the asymptotic values $\beta_g^*(s \rightarrow \infty) = 0.564$ and $\beta_\sigma^*(s \rightarrow \infty) = 0.387$ are almost reached if $s > 100$. The ratio β_g^*/β_σ^* is almost constant over the whole range of s considered. Both functions tend to zero at the same $s^* = 1.305$. While in the parameter region below the curve $\beta_g^*(s)$ the flow destabilizes the interface for perturbations with wave numbers $0 \leq \beta \leq \beta_g^*(s)$ the interface is stabilized by the flow above as $\beta \geq \beta_g^*(s)$.

For strong remote flow it makes no sense to display only deviations from the no flow stability results since they may reach the same order of magnitude. Therefore the neutral curves $M^{-1}(\beta)$ for several values of $P = 0, 1, 10$ are plotted directly in figure 12. The viscous layer thickness has been fixed by setting $s = 1$. Results for $P > 10$ are not displayed since a good approximation with the truncated power series would require more than 10 terms. The results show that the flow is monotonically stabilized with increasing magnitude of the fluid velocity. For flows with $P = 10$ the critical value of $M_c^{-1} = 0.073$ is by a factor of 3.66 times smaller than that at $P = 0$. This allows e.g. the use of significantly lower temperature gradients or higher pulling velocities while the interface still remains stable.

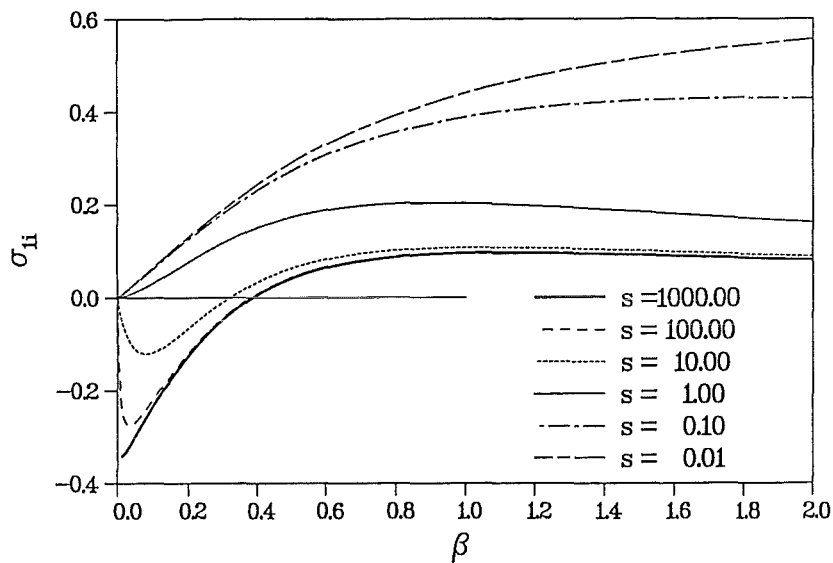


Figure 10: Imaginary part σ_i of the complex growth rate at marginal stability, induced by weak remote parallel shear flow, versus the morphological wave number β for different values of s .

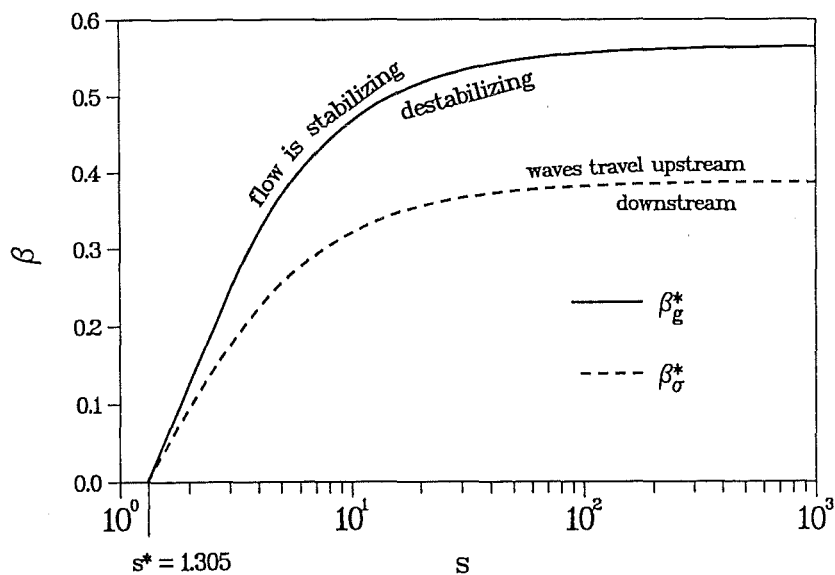


Figure 11: β_g^* and β_σ^* versus s . The wave numbers $0 < \beta < \beta_g^*$ are destabilized by the remote flow. Below $s^* = 1.305$ there is no destabilized window of wave numbers and perturbations with any wave number travel upstream.

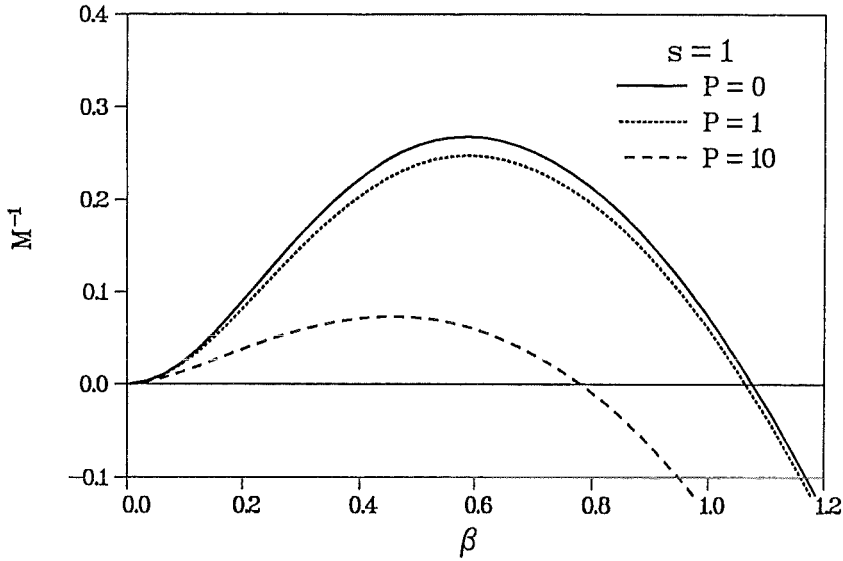


Figure 12: Marginal stability of the stationary interface for $s = 1$ and $P = 0, 1, 10$. M^{-1} versus β for $k = 0.3$ and $\Gamma = 0.6$.

4.2.2 $\alpha\xi$ -periodic flows

Consider now the case of a remote flow periodic in $\alpha\xi$, through the flow amplitude $P(\alpha\xi)$. The linear stability problem is obtained by writing the solutions in temporal normal modes where the deformation of the interface is expressed as

$$H = H_0 + \varepsilon H_1 e^{\sigma\tau} \quad (89)$$

and the solution in the other variables is written according to

$$\begin{pmatrix} \omega \\ \psi \\ c \end{pmatrix} = \begin{pmatrix} \omega_0 \\ \psi_0 \\ c_0 \end{pmatrix} + \varepsilon \begin{pmatrix} \omega_1 \\ \psi_1 \\ c_1 \end{pmatrix} e^{\sigma\tau} \dots \quad (90)$$

The unknowns are expanded with the small wave number α of the flow field as

$$\begin{pmatrix} \omega_1 \\ \psi_1 \\ c_1 \end{pmatrix} = \begin{pmatrix} \omega_{10} \\ \psi_{10} \\ c_{10} \end{pmatrix} + \alpha \begin{pmatrix} \omega_{11} \\ \psi_{11} \\ c_{11} \end{pmatrix} + \dots, \quad (91)$$

where the variables ω_1, ψ_1, c_1 depend on ξ and ζ . It would be convenient to use the fact that α is small in a straight-forward perturbation scheme, but the product $\alpha\xi = \eta$ in P is non-uniform. When $\alpha \rightarrow 0$, η may be any value. This situation suggests that one instead use a WKB representation for small α .

The equation at $O(\varepsilon, \alpha^0)$ with $\eta = O(1)$ then reads:

$$\zeta^2 c_{10\zeta\zeta} + c_{10\xi\xi} - P(\eta)\zeta\psi_{0\zeta}c_{10\xi} - \sigma c_{10} = \zeta(\sigma H_1 - H_{1\xi\xi} - \psi_{10\xi}), \quad (92)$$

where $c_0 = \zeta + O(\alpha)$ has been used already. The solution vanishes at infinity, $c_{10} = 0$ at $\zeta = 0$ and the interface conditions at $\zeta = 1$ are

$$c_{10} = -M^{-1}H_1 + \Gamma H_{1\xi\xi} \quad (93)$$

and

$$c_{10\zeta} + c_{10}(k-1) = -\sigma k H_1. \quad (94)$$

Further a solution is assumed for c_{10} according to a power series in ζ as

$$c_{10}(\xi, \zeta) = -\zeta H_1(\xi) + \sum_{\nu=0}^{\infty} C(\xi)_{\nu} \zeta^{\mu+\nu/s}. \quad (95)$$

After collecting like powers one obtains for $\nu = 0$:

$$C_{0\xi\xi} - P(\eta)C_{0\xi} + \beta_0^2 C_0 = 0, \quad (96)$$

where the abbreviation $\beta_0^2 = \mu^2 - \mu - \sigma$ has been used. If there were no flow, $P = 0$, the first element C_0 in the power series would satisfy the equations already exactly. The value of β_0 then corresponds to the pure morphological wave number. If a periodic remote flow is present solutions are found by using WKB techniques. If one writes

$$C_0 = e^{\phi(\eta)/\alpha} \quad (97)$$

in the equation (96) and higher order terms in α are neglected one finds

$$\phi_{1,2} = \frac{1}{2} \int \left(P(\eta) \pm \sqrt{P(\eta)^2 - 4\beta_0^2} \right) d\eta, \text{ where } \eta = \alpha\xi. \quad (98)$$

Up to this point the structure of the flow along η has not been specified yet. In the following our attention is restricted to the case where $P(\eta)$ is proportional to a harmonic function

$$P(\eta) = -\hat{P} \sin \eta. \quad (99)$$

The amplitude \hat{P} is assumed to be positive and the sign has been introduced for convenience. With this notation the position $\eta = 0$ is a 'converging' stagnation point. Now the solution for ϕ is given by

$$\phi_{1,2} = \frac{1}{2} \hat{P} \cos \eta \pm iE \left(\eta, \frac{\hat{P}}{2\beta_0} \right) \beta_0 \quad (100)$$

where $E \left(\eta, \frac{\hat{P}}{2\beta_0} \right)$ is the *elliptic integral of the second kind* with modulus $\frac{\hat{P}}{2\beta_0}$ [3]. The solution for C_0 is determined and reads up to an arbitrary multiplicative constant

$$C_0 = e^{\frac{1}{2} \frac{\hat{P}}{\alpha} (\cos \eta - 1)} \cos \left(\beta_0 \frac{E \left(\eta, \frac{\hat{P}}{2\beta_0} \right)}{\alpha} \right). \quad (101)$$

This solution has been obtained assuming zero flux conditions with $C_{0\eta} = 0$ at $\eta = 0$ and at $\eta = 2\pi$ and by assuming that the solution over the whole period remains finite

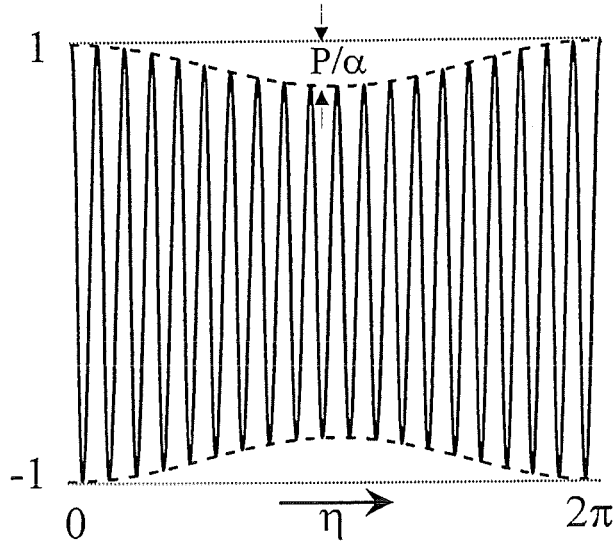


Figure 13: Sketch of the interface at marginal stability for a weak flow. The periodic deformation is slightly modulated on the scale of the flow with higher values near the converging stagnation points.

as $\alpha \rightarrow 0$. The zero flux condition here is equivalent to the more general conditions for periodicity with $\eta = 2\pi$, when symmetry with respect to $\eta = 0$ and $\eta = 2\pi$ is assumed.

For very weak flows ($\hat{P}/\alpha \ll 1$) the solution becomes

$$C_0 = \cos(\beta_0 \xi) \left[1 + \frac{1}{2} (\cos \eta - 1) \frac{\hat{P}}{\alpha} + O\left(\left(\frac{\hat{P}}{\alpha}\right)^2\right) \right]. \quad (102)$$

The solution is similar to the no-flow case, $\cos(\beta_0 \xi)$. The influence of the weak flow is reflected in the small modulation on the long scale of the flow with $\cos \eta$. A sketch of this quasi-parallel solution is shown in figure 13.

If the flow magnitude is $\hat{P} = O(1)$, the solution for the concentration exhibits boundary layers near $\eta = 0, 2\pi, \dots$, while the solution is exponentially small in the rest of the η domain as $\alpha \rightarrow 0$. It can be easily shown that the solution then takes the form

$$C_0 = \cos(\beta_0 \xi) e^{-\frac{1}{4} X^2} \quad (103)$$

where $X = \sqrt{\hat{P}/\alpha} \eta = \sqrt{\alpha \hat{P}} \xi$ is the properly rescaled slow coordinate near the stagnation point (here at $\eta = 0$). Again a solution is found similar to the no-flow case, now modulated with a Gaussian envelope. The sinusoidal solution exist with relevant amplitude only in the vicinity of the *converging* stagnation points at $\eta = 0, 2\pi, \dots$ in a region of width of the order $(\alpha/\hat{P})^{1/2}$, highly localized with respect to the long wave length of the flow. Near the *diverging* stagnations points $\eta = \pi, 3\pi, \dots$ the solution remains exponentially small as in the rest of the η domain (see figure 14).

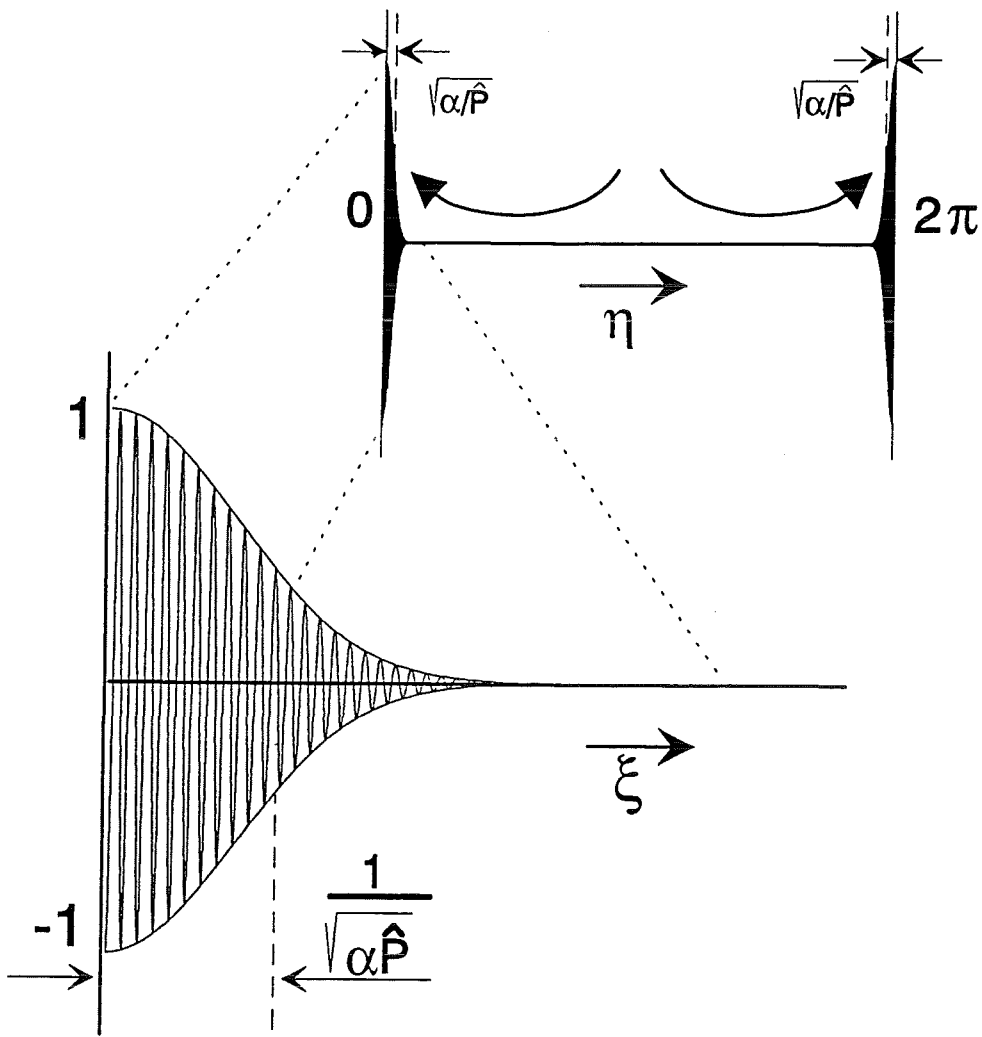


Figure 14: Sketch of the interface for a flow of order one. On the scale η of the flow the deformation of the interface is exponentially small over almost the whole period, except in thin regions of width $(\alpha/\hat{P})^{1/2}$. There the morphological instability is present, modulated by a Gaussian envelope.

The solutions for the proceeding orders in ν are obtained by a successive solution of the equations

$$C_{(\nu)\xi\xi} - P(\eta)C_{(\nu)\xi} + \beta_\nu^2 C_{(\nu)} = -P(\eta)C_{(\nu-1)\xi}. \quad (104)$$

It can be shown that for both cases according to equations (102,103) the contributions $C_{(\nu)}$ with $\nu \geq 1$ become negligibly small as $\alpha \rightarrow 0$. Therefore, the solution for the perturbation of the concentration is well represented by the first term in the power series in equation (95).

Substituting these results into the equilibrium condition at the interface leads to an equation determining the interface deformation H_1 .

$$\Gamma H_{1\xi\xi} + (1 - M^{-1}) H_1 = C_0. \quad (105)$$

It can be shown that the solution

$$H_1 = \frac{C_0}{g} \quad (106)$$

with $g = 1 - M^{-1} - \Gamma\beta_0^2$ satisfies the equilibrium condition in the limit $\alpha \rightarrow 0$.

If the results above are introduced into the equation for conservation of solute one finds the result that

$$g = \frac{k}{1 - k - \mu} \quad (107)$$

at marginal stability. This result is the same as already obtained for the case with no flow given in equation (43). The threshold for instability is not affected by the imposed remote flow if $\alpha \ll 1$. This result is not surprising at this point since neither the leading-order solution for the concentration field nor the interface deformation depend directly on the magnitude of the flow. Even if the flow had globally an $O(1)$ magnitude its values near the stagnation points where the solution is localized is negligibly small and thus does not at all affect the stability boundaries.

For completeness of the analysis it should be noted that after inserting the ansatz for the concentration into the equation (92) there remain terms depending in ζ which contain factors that are not direct multiples of $\zeta^{\mu+\nu/s}$. These terms can be expanded in the similar power series as used for the concentration, if desired. It can be shown that all these additional terms are multiplied by $\hat{P}(\eta)H_{1\xi}$. Knowing that H_1 is mainly proportional to C_0 the additional terms can be incorporated easily in the equation (96). The final result may be altered in such a way that the magnitude of the periodic coefficient changes from \hat{P} to \hat{P}' and the appropriate coordinate describing the decay of the localized concentration pattern becomes $X = \sqrt{\alpha\hat{P}'}\xi$. Qualitatively the solution remains unchanged. The highly localized structures are still formed and the remote flow has no influence on the marginal limit of stability as $\alpha \rightarrow 0$.

5 Numerical solution

In order to confirm the results obtained above numerical calculations are performed applying finite difference methods on the original nonlinear equation (27) for the concentration. The induced flow has been neglected for the present analysis. To keep the variables in reasonable order of magnitude, say $O(1)$ during the numerical calculations, the concentration c and the interface deformation H , but also the Laplacian \mathbb{L} are replaced by

$$\begin{pmatrix} c(\xi, \zeta, \tau) \\ H(\xi, \tau) \\ \mathbb{L} \end{pmatrix} \rightarrow \begin{pmatrix} \zeta \\ \zeta \partial_\zeta \end{pmatrix} + \begin{pmatrix} c_0(\xi, \zeta) \\ H_0(\xi) \\ \mathbb{L}_0 \end{pmatrix} + \varepsilon \begin{pmatrix} c(\xi, \zeta, \tau) \\ H(\xi, \tau) \\ \mathbb{L}_1 \end{pmatrix} + \varepsilon^2 \begin{pmatrix} \\ \\ \mathbb{L}_2 \end{pmatrix} \quad (108)$$

with

$$\begin{aligned} \mathbb{L}_0 &= \partial_{\xi\xi} + \zeta^2 (1 + H_{0\xi}^2) \partial_{\zeta\zeta} + \zeta (H_{0\xi}^2 + H_{0\xi\xi}) \partial_\zeta + 2\zeta H_{0\xi} \partial_{\xi\zeta}, \\ \mathbb{L}_1 &= 2\zeta^2 H_{0\xi} H_\xi \partial_{\zeta\zeta} + \zeta (2H_{0\xi} H_\xi + H_{\xi\xi}) \partial_\zeta + 2\zeta H_\xi \partial_{\xi\zeta}, \\ \mathbb{L}_2 &= H_\xi^2 (\zeta^2 \partial_{\zeta\zeta} + \zeta \partial_\zeta). \end{aligned} \quad (109)$$

The variables c_0 and H_0 describe the deviations of the stationary solution from the uniform basic state which would establish if there were no flow in the liquid phase. Their solution may be obtained from the equation in the leading order

$$\zeta (\psi_\zeta c_{0\xi} - \psi_\xi c_{0\zeta}) = \zeta \psi_\xi + \mathbb{L}_0 (\zeta + c_0) \quad (110)$$

with the appropriate boundary conditions. It has been shown in chapter 4.1, that c_0 and H_0 are proportional to $\alpha/(1+s)$ and vanish like ψ_ξ in the limit considered,

$$c_0 = H_0 = \psi_\xi = 0 \text{ as } \alpha \rightarrow 0. \quad (111)$$

This leads to considerable simplifications of the equation (27) which becomes

$$c_\tau + \zeta \psi_\zeta c_\xi = \mathbb{L}_0 c + \zeta (H_{\xi\xi} - H_\tau) + \varepsilon [\mathbb{L}_1 c + \zeta (H_\xi^2 - H_\tau c_\zeta)] + \varepsilon^2 \mathbb{L}_2 c \quad (112)$$

governing the time dependent non-linear solution of the concentration.

At infinity, $\zeta = 0$, the concentration vanishes, $c = 0$. The equilibrium condition and the conservation of solute at the interface $\zeta = 1$ require that

$$c = -M^{-1}H + \Gamma H_{\xi\xi}, \quad (113)$$

$$H_\tau = \frac{c_\zeta - (1-k)c + \varepsilon (H_\xi c_\xi + H_\xi^2) + \varepsilon^2 H_\xi^2 c_\zeta}{1 + \varepsilon(1-k)c}. \quad (114)$$

The departure of the morphological number from the stability limit determines the value of ε if $M^{-1} = M_c^{-1}(1 + \varepsilon^2)$. Note that for $\varepsilon = 0$ the equations (112-114) describe the linear stability problem. The critical value M_c^{-1} is the number for which the eigenfunctions c and H do not change in time. For $\varepsilon > 0$ the nonlinear time-dependent problem is recovered.

All spatial derivatives are approximated by second-order finite differences. The equation (112) is integrated in time using a ADI scheme for the spatial directions ξ and ζ by a Fortran subroutine described in [2]. The equation (114) describing the conservation of solute is advanced in time using an explicit Euler scheme.

5.1 Linear stability

To ensure a direct comparison with the analytical results the same assumptions are used for the numerical calculations. The linear stability results are obtained by advancing the equations (112, 114) in time for $\varepsilon = 0$, normalizing the maximum amplitude of the interface perturbation at each time step. The normalization factor leads directly to the linear growth rate. Calculations are performed using the same parameters as for the analytical results $k = 0.3$, $\Gamma = 0.6$. It is assumed that the system is at marginal stability with $M_c^{-1} = 0.267$, $\beta_c = 0.582$ according to the analytical predictions. The ξ -direction is resolved with $n_\xi = 20$ points per morphological wave length, the ζ direction with $n_\zeta = 10$. Test calculations using this grid showed that deviations for the critical parameter M_c^{-1} from the analytical predictions are smaller than 0.5% for the no-flow case. For cases with flow, the stream function is given as $\psi = -\hat{P} \sin(\eta) (s + \ln s - s\zeta^{1/s})$, where $\eta = \alpha\xi$. The velocity component normal to the interface ψ_ξ is neglected compared to the tangential one, assuming $\alpha \ll 1$. The computational domain is chosen long enough that a high number n of morphological modes fit into one wave length of the flow, $\alpha = \beta_c/n$. Calculations are performed using a half period of the flow $0 \leq \eta \leq \pi$ with homogeneous Neumann conditions at $\eta = 0$ and at η_{\max} , due to symmetry, or using a full period $0 \leq \eta \leq 2\pi$, assuming cyclic conditions. Most of the results displayed below have been checked using several initial conditions.

It is expected that a comparison with the analytical solution should become better, the higher the number of morphological modes n , which fit within one wave length of the flow, would be. First, $n = 1000$ modes are used between $0 \leq \eta \leq 2\pi$. This requires 10000 grid points tangential to the interface to resolve the computational interval $0 \leq \eta \leq \pi$, which corresponds to $0 \leq \xi \leq 5400$. For the parameters $\Gamma = 0.6$, $\hat{P} = 0.1$, $s = 100$, and $\alpha = \beta_c/1000$ results are displayed in figure. The interface pattern is located near the converging stagnation point as predicted by the analytical solution. The solution displayed in figure 15 is the result after an integration time of $\tau = 10^4$. The calculation was started using a perturbation at this stagnation point. The width of the unstable pattern first expanded towards larger values of η but finally decreased to the solution shown in the plot. During the last period of integration, $5 \cdot 10^3 < \tau < 10^4$, the width of the localized pattern did not change more than about 1%. The numerical solution exhibits a strong tendency to keep this solution for a very long time. This gives some confidence in a comparison with the analytical predictions. The analysis predicts an envelope proportional to

$$e^{-\left(\frac{n}{\eta_0}\right)^2} = e^{-\left(\frac{\xi}{\xi_0}\right)^2}. \quad (115)$$

With this notation it becomes clear that the width of the solution is small enough on the η -scale to be called localized, $\eta_0 = 2 \left(\alpha/\hat{P}\right)^{1/2} = 0.15$, but large enough on the ξ -scale to have a good number of morphological modes with significant amplitude since $\xi_0 = 2 \left(\alpha\hat{P}\right)^{-1/2} = 262.2$. For a comparison the analytically obtained envelope is plotted in the figure together with the numerical solution.

The results obtained so far indicate that a good comparison with the analytical predictions is possible for very small values of α .

Further tests, however, showed that the restriction on α alone is not enough in order

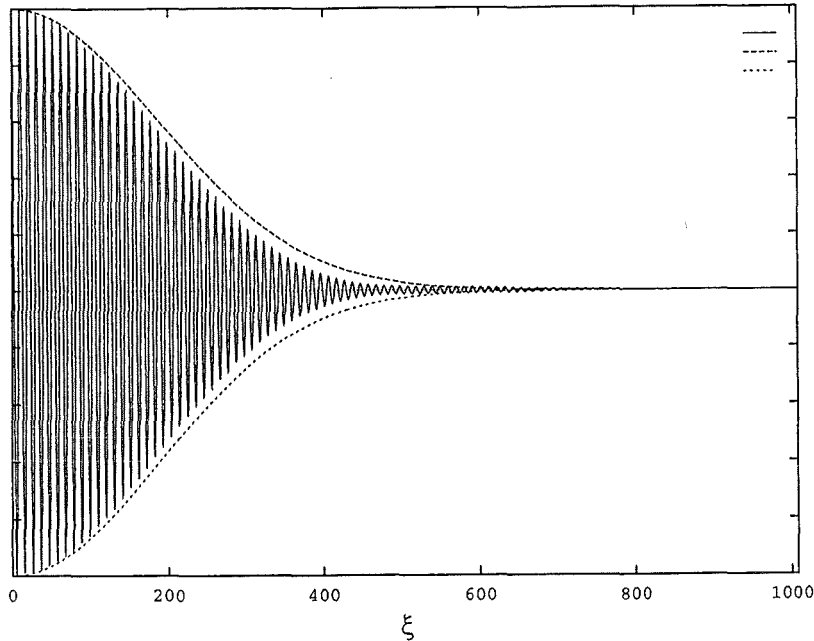


Figure 15: Stationary interface pattern near the converging stagnation point for $\Gamma = 0.6$, $k = 0.3$, $\hat{P} = 0.1$, $s = 100$, $n = 1000$. The envelope according to the analytical prediction is plotted in the figure for comparison.

to find a good agreement. There exists in addition a restriction on \hat{P} . This has been demonstrated by using $\hat{P} = 10$, a value which is 100 times larger than the previous one. With this value the solution first showed the expected behavior, but after some integration time the maximum amplitude was no longer located near the stagnation point. It started to move towards a position between the stagnation points. This may be explained by the fact that during the analytical solution terms of the order $O(\alpha\hat{P})$ were neglected. A good comparison therefore requires not only that $\alpha \ll 1$ but that $\alpha\hat{P} \ll 1$. Similar patterns are obtained if α is not sufficiently small, as will be outlined in the following.

Next, the results are discussed for $\hat{P} = 1$, $s = 10$, and $n = 100$, a flow of order one with moderate thickness of the viscous layer. Unlike the analytical prediction the fastest growing solution is not located at the converging stagnation points at $\eta = 0$ and $\eta = 2\pi$. Moreover, all numerical predictions indicate, that the solution is located in the regions with the strongest tangential velocities, near $\eta = \frac{1}{2}\pi$ and near $\eta = \frac{3}{2}\pi$ see figure 16. While the interface pattern obtained as the analytical solution were stationary, they are travelling here with the direction of the flow. They travel to the left, for $0 \leq \eta \leq \pi$ and to the right for $\pi \leq \eta \leq 2\pi$. Small perturbations are transported with the flow and amplified along their path. After they have passed the location of the velocity maximum, they are damped. They become negligible before they reach the stagnation point. One reason why the patterns are more stable near the stagnation points is the fact that they are stretched or compressed near the diverging or the converging stagnation points, respectively. This changes their wave number so that the local β becomes larger or smaller than the critical value for the morphological instability; the interface is locally stabilized. Between two stagnation points there exists a region where the velocity is almost constant. The interface pattern is advected mainly, with unchanged wave length.

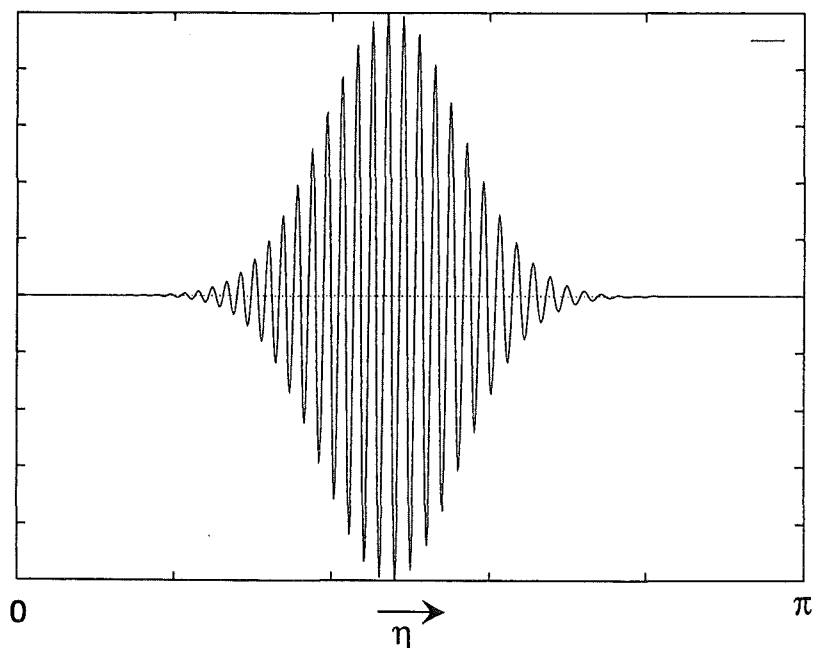


Figure 16: Interface pattern $H(\eta, \tau)$ after all transitions are completed for $\Gamma = 0.6$, $k = 0.3$, $\hat{P} = 1$, and $s = 10$, $\alpha = \beta/100$. The displayed interface pattern is travelling from the diverging stagnation point at $\eta = \pi$ towards the converging stagnation point at $\eta = 0$ in $-\xi$ -direction, while the envelope remains stationary. Between $\eta = \pi$ and $\eta = 2\pi$ the same situation is found; there the pattern travels in the $+\xi$ -direction.

This may allow solutions growing faster near $\eta = \frac{1}{2}\pi$ and near $\eta = \frac{3}{2}\pi$ than near the stagnation points. Remember, that for the actually used parameters a parallel shear flow should stabilize the interface compared to the no-flow case (see e.g. figure 11). In dead, the numerical calculations predict a maximum growth rate $\sigma_r < 0$ with flow for a parameter combination that would lead to $\sigma = 0$ if there were no flow. *The flow is stabilizing.* However, the stretching and compression of the pattern near the stagnation points produces a stronger stabilization.

Similar solutions are obtained for weaker flows near the interface. In figure 17 the flow is still of order one, $\hat{P} = 1$, but now the viscous layer is ten times thicker than in the previous case, $s = 100$. The stretching and compression of the pattern near the stagnation points is weaker, as well as the damping of the fastest growing mode. The wavy interface shape extends over larger ranges. A peculiar situation is reached for the again weaker flow with $\hat{P} = 0.1$, $s = 100$ as shown for a fixed time in figure 18. The interface perturbations reach the stagnation points. The stretching or compression is now so weak, that the waves have enough time to develop visible amplitudes at $\eta = 0$ and at $\eta = \pi$. However, after some more computational time their wave length near the stagnation points becomes again inadequate and they vanish there. The solution then looks very similar to figure 17. The solution vanishes temporarily near the stagnation points. During some transition time, the solution near the stagnation points grows again, now having one additional mode near the diverging and one mode less near the converging stagnation point. This performance repeats (at least as long as it has been calculated; four times within a computational time of $\tau = 6 \cdot 10^4$, starting with random initial conditions). This behavior is illustrated in a H contour plot in the η - τ -

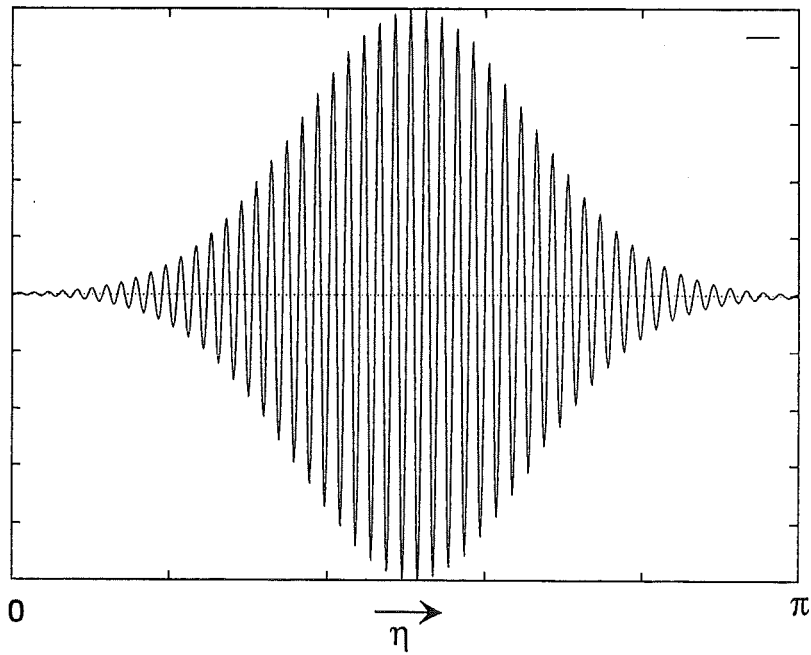


Figure 17: Interface pattern $H(\eta, \tau)$ after all transitions are completed for $\Gamma = 0.6$, $k = 0.3$, $\hat{P} = 1$, $s = 100$, $\alpha = \beta_c/100$.

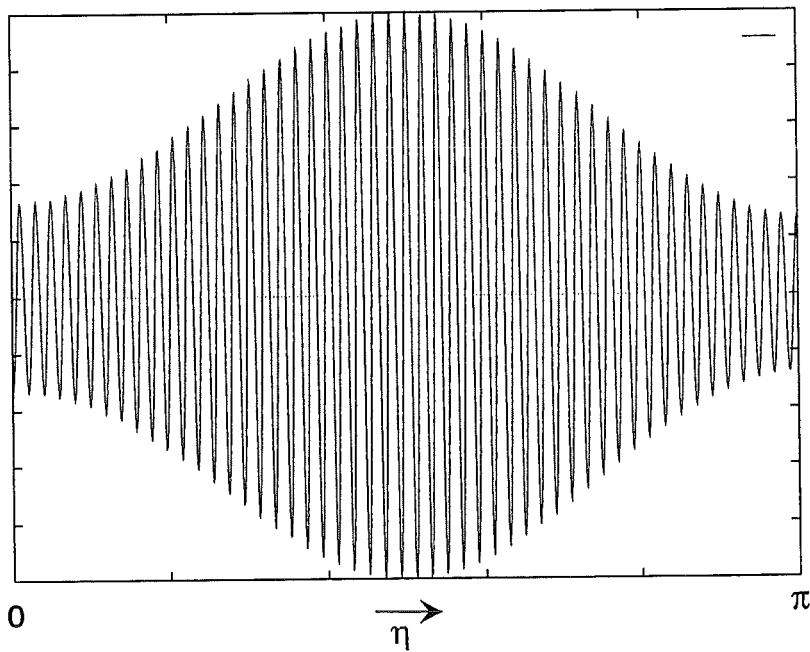


Figure 18: Interface pattern $H(\eta, \tau)$ after all transitions are completed for $\Gamma = 0.6$, $k = 0.3$, $\hat{P} = 0.1$, and $s = 100$, $\alpha = \beta_c/100$.

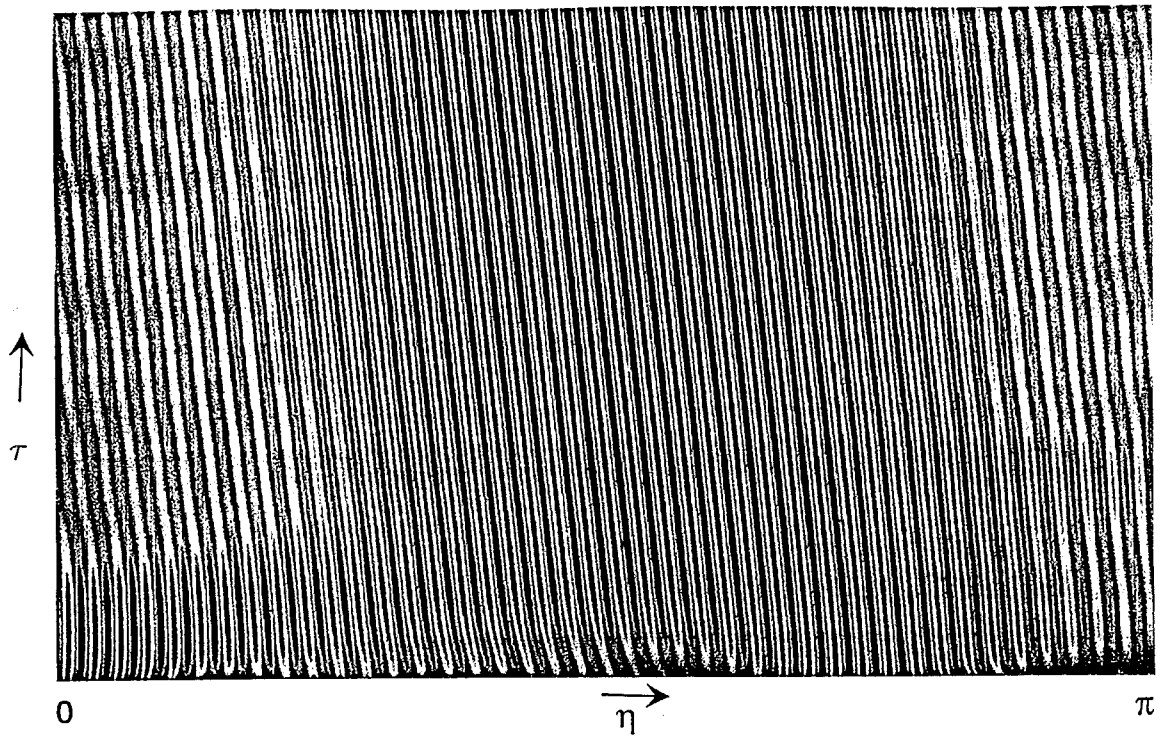


Figure 19: Contour plot of $H(\eta, \tau)$. Starting from random initial conditions at $\tau = 0$ the solution of the interface pattern develops in time. The periodic interface pattern is mainly located between the stagnation points. During regular time intervals the solution near the stagnation points vanish. This allows a reorganization of the pattern in these regions. One additional mode is created near the diverging, another mode is eliminated near the converging stagnation point. The inclination of the contour levels in the ξ - τ - plane gives the traveling speed of the pattern in the region between the stagnation points.

plane as shown in figure 19.

The numerical solutions can differ from the analytical ones because the number of $n = 100$ morphological modes per wave length of the flow is not high enough to get a good comparison with the asymptotic solution where terms of the order α or $\alpha\hat{P}$ have been neglected. The region near the stagnation point within which the localized solution would be expected is too small. There are too few modes near the stagnation points and the stretching and compression acts strongly upon them. This point of view is supported by the observation that for small enough α the numerical and analytical solutions are comparable.

6 Conclusions

In this paper the stability of a stationary solid-liquid interface is considered in unidirectional solidification of a dilute binary alloy. The liquid and solid phases are assumed to have equal density and heat conductivity. The problem is simplified by using the frozen temperature approximation and by considering only materials with very large Schmidt numbers. At the interface thermodynamic equilibrium is assumed taking into account capillary and constitutional undercooling. When results are displayed they refer to a system lead-tin with $k = 0.3$ and $\Gamma = 0.6$ [17].

Firstly, a solidification problem is solved in which a flow in the liquid phase is driven by weak solutal buoyancy in a gravitational field aligned with the pulling direction of the crystal. The flow is governed by a baroclinic motion above the curved interface. If the interface remains planar the flow will come to a rest. The main result here is that a weak solutal buoyant flow stabilizes the planar interface, compared to the no-flow case, for values of the solutal Rayleigh number $R > 0$ while the flow destabilizes the interface for $R < 0$. The magnitude of the (de-)stabilization is expressed in terms of corrections g_1 to the control parameter M^{-1} , the inverse morphological number. The flow pattern is discussed in detail especially for small wave numbers α of the flow.

Secondly, a stability problem is analyzed, in which a stationary interface is subjected to a remote flow in the liquid phase. The remote flow has been assumed to be given, e.g. as locally parallel flow with magnitude P far from the interface. The flow decays exponentially towards the interface across a viscous layer of thickness s . These two parameters characterize a whole class of velocity profiles and have important influence on the results. The perturbation concentration is approximated by a truncated generalized power series in ζ , along the direction normal to the interface. Each element in this series represents an exponential in z . Such an approximation seems to be very efficient for weak flows, since the first term alone satisfies already the no-flow equations exactly. Nevertheless, the analysis is not restricted to weak flows only, since stronger flows can be considered as well by using a larger number of terms in the approximation. For weak parallel remote flow it turns out, that changes of the control parameter due to the flow are proportional to δ^2 , where $\delta = P/(1+s)$. Near the interface, within an $O(1)$ distance, this parameter represents the magnitude of the tangential velocity if $s \ll 1$ or the constant velocity gradient if $s \gg 1$. The flow field far from the interface is of negligible importance. For very thin viscous layers, $s \ll 1$, the flow stabilizes the interface over the whole range of morphological wave numbers β . For $s > s^* = 1.305$ there exists a band of wave numbers within which the flow destabilizes the stationary solution. The strongest destabilization is observed when β^{-1} becomes comparable to s , when the wave length becomes of similar size as the thickness of the viscous layer. The range of destabilizing wave numbers depends on s and may reach maximal extension from $\beta = 0$ to 0.564 as $s \rightarrow \infty$. All higher wave numbers are stabilized by the flow for all s . At the onset of instability the linear theory predicts travelling waves, the direction of which is related to the direction of the flow. While for flows with $s < s^*$ waves with any wave number considered move against the direction of the imposed flow there exist a band of wave numbers within which the waves move with the flow as $s > s^*$. The results have been checked by comparison with special solutions known from literature. While all these results have been obtained assuming that $\delta \ll 1$, it is shown in addition

that the theory is capable of treating cases with $\delta = O(1)$ or larger.

Thirdly, analysis was made of the influence of flows which have a spatially periodic pattern $P(\alpha\xi) = \hat{P}e^{i\alpha\xi}$ like those that arise in the case of solutal buoyancy at small α . It has been assumed that the wave number α of the flow is much smaller than the morphological wave number β at which the instability would occur. For periodic remote flows the stationary interface no longer remains planar. The flow induces periodic spatial variations in the concentration field, which lead to a deformation of the steady state interface. It is shown that the parameter δ controls the magnitude of the stationary interface deformation. A linear stability analysis finds at leading order in α , $\alpha \ll 1$, that spatially periodic remote flows do not affect the critical values for the onset of instabilities compared to the situation when no flow is present. However, at the onset of instability the temporally growing solutions for the concentration and for the interface deformation are highly localized in the narrow vicinity of the converging stagnation points and are exponentially small over the rest of the wave length of the flow. It is shown that the width of the localized pattern on the scale of the flow $\eta = \alpha\xi$ is $\eta_0 \sim (\alpha/\hat{P})^{1/2}$, a value which vanishes as α tends to zero. On the scale of the morphology, say on ξ , the width of the localized pattern is $\xi_0 \sim (\alpha\hat{P})^{-1/2}$. These two results demonstrate the possibility that for small enough values of α the pattern should be highly localized on the scale of the flow, but on the other hand on the scale of the morphology the pattern is still wide enough to allow a large number of morphological modes near the stagnation points.

A comparison of analytically obtained results with numerical predictions showed good agreement if the product $\alpha\hat{P}$ is sufficiently small. For a value of $\alpha = \beta_c/1000$ and $\hat{P} = 0.1$ the numerical and analytical results find approximately the same width of the localized interface pattern. Numerical computations which do not ensure the smallness of $\alpha\hat{P}$ lead to qualitatively different interface pattern at the onset of the morphological instability. If $\alpha\hat{P}$ is small, but not small enough, the temporally growing instabilities are no longer localized near the converging stagnation points. Moreover, their magnitude vanishes at the stagnation points. The highest amplitude is found at positions between stagnation points where the highest tangential speeds occur. The eigenfunctions are amplitude-modulated waves travelling with the flow. They are travelling to both directions simultaneously within one wave length of the flow. Such a behavior may find the following explanation: Near the stagnation points the interface patterns are stretched or compressed by the fluid motion. This increases or decreases locally the wave number and draws the solution in these regions back to a more stable regime than without flow. Between the stagnation points the interface pattern is mainly advected by the flow, leaving the wave number unchanged. Also in these regions the flow acts stabilizing on the interface like in the case of locally parallel shear flow. However, the stabilization here is much weaker than the previously mentioned stabilization due to a change in the local wave numbers near the stagnation points so that the fastest growing modes are found in the regions of highest, almost uniform tangential velocities. Such results can not be compared with analytical findings since one of the basic assumptions during the derivation of the analytical results was that $\alpha \rightarrow 0$ or that $\alpha\hat{P} \ll 1$. Nevertheless, these results display what is going on for parameter combinations beyond the assumptions of the analysis.

Acknowledgment

This work began while S. H. Davis was the holder of a senior Von Humboldt research award in residence at the Forschungszentrum Karlsruhe. He gratefully acknowledges the hospitality of the Forschungszentrum Karlsruhe and its Institute for Applied Thermo- and Fluidynamics.

The work was continued during the delegation of L. Bühler to the Northwestern University in Evanston, Chicago which was made possible by a Post Doctoral Fellowship at the department of Engineering Science and Applied Mathematics.

References

- [1] K. Brattkus and S. H. Davis. Flow induced morphological instabilities: Stagnation-point flow. *Journal of Crystal Growth*, 89:423–427, 1988.
- [2] L. Bühler. Convective-diffusive transport in laminar mhd flows. Technical Report 5241, KfK, September 1993.
- [3] P. F. Byrd and M. D. Friedman. *Handbook of elliptic integrals for engineers and scientists*. Springer, 1971.
- [4] S. R. Coriell, M. R. Cordes, W. S. Boettinger, and R. F. Sekerka. Convective and interfacial instabilities during unidirectional solidification of a binary alloy. *Journal of Crystal Growth*, 49:13–28, 1980.
- [5] S. R. Coriell and G. B. McFadden. Buoyancy effects on morphological instability during directional solidification. *Journal of Crystal Growth*, 94:513–521, 1989.
- [6] S. R. Coriell and G. B. McFadden. Morphological stability. In D. T. J. Hurle, editor, *Handbook of Crystal Growth 1*, volume 1, chapter 12, pages 787–858. Elsevier Science Publishers, 1993.
- [7] S. R. Coriell, G. B. McFadden, and R. F. Boisvert. Effect of a forced couette flow on coupled convective and morphological instabilities during unidirectional solidification. *Journal of Crystal Growth*, 69:15–22, 1984.
- [8] S. H. Davis. Effects of flow on morphological stability. In D. T. J. Hurle, editor, *Handbook of Crystal Growth 1*, volume 1, chapter 13, pages 861–897. Elsevier Science Publishers, 1993.
- [9] R. T. Delves. Theory of the stability of a solid-liquid interface during growth from stirred melts. *Journal of Crystal Growth*, 3,4:562–568, 1968.
- [10] S. A. Forth and A. A. Wheeler. Hydrodynamic and morphological stability of the unidirectional solidification of a freezing binary alloy: a simple model. *Journal of Fluid Mechanics*, 202:339–366, 1989.
- [11] A. K. Hobbs and P. Metzener. Long-wave instabilities in directional solidification with remote flow. *Journal of Crystal Growth*, 112:539–553, 1991.
- [12] D. T. J. Hurle, E. Jakeman, and A. A. Wheeler. Effect of solutal convection on the morphological stability of a binary alloy. *Journal of Crystal Growth*, 58:163–179, 1982.
- [13] D. T. J. Hurle, E. Jakeman, and A. A. Wheeler. Hydrodynamic stability of the melt during solidification of a binary alloy. *Physics of Fluids*, 26(3):624–626, 1983.
- [14] J. S. Langer. Instabilities and pattern formation in crystal growth. *Review of Modern Physics*, 52(1):1, 1980.

- [15] G. J. Merchant and S. H. Davis. Shallow cells in directional solidification. *Physical Review Letters*, 63(5):573575, 1989.
- [16] W. W. Mullins and R. F. Sekerka. Stability of a planar interface during solidification of a dilute binary alloy. *Journal of Applied Physics*, 35(2):444, 1964.
- [17] T. P. Schulze and S. H. Davis. The influence of oscillatory and steady shear on interfacial stability during directional solidification. *Journal of Crystal Growth*, 143:317–333, 1994.
- [18] G. W. Young and S. H. Davis. Directional solidification with buoyancy in systems with small segregation coefficient. *Physical Review B*, 34(5):3388, 1986.